Hot new early dark energy bridging cosmic gaps:
Supercooled phase transition reconciles stepped dark radiation
solutions to the Hubble tension with BBN

Mathias Garny[1,*], Florian Niedermann[2,†], Henrique Rubira,[1,‡] and Martin S. Sloth[3,§]

[1]*Physik Department T31, Technische Universität München*
James-Franck-Straße 1, D-85748 Garching, Germany
[2]*Nordita, KTH Royal Institute of Technology and Stockholm University,*
Hannes Alfvéns väg 12, SE-106 91 Stockholm, Sweden
[3]*Universe-Origins, University of Southern Denmark, Campusvej 55, 5230 Odense M, Denmark*

We propose a simple model that can alleviate the H_0 tension while remaining consistent with big bang nucleosynthesis (BBN). It is based on a dark sector described by a standard Lagrangian featuring a $SU(N)$ gauge symmetry with $N \geq 3$ and a massive scalar field with a quartic coupling. The scalar acts as a dark Higgs leading to spontaneous symmetry breaking $SU(N) \to SU(N-1)$ via a first-order phase transition *à la* Coleman-Weinberg. This setup naturally realizes previously proposed scenarios featuring strongly interacting dark radiation (SIDR) with a mass threshold within hot new early dark energy. For a wide range of reasonable model parameters, the phase transition occurs between the BBN and recombination epochs and releases a sufficient amount of latent heat such that the model easily respects bounds on extra radiation during BBN while featuring a sufficient SIDR density around recombination for increasing the value of H_0 inferred from the cosmic microwave background. Our model can be summarized as a natural mechanism providing two successive increases in the effective number of relativistic degrees of freedom after BBN but before recombination $\Delta N_{\mathrm{BBN}} \to \Delta N_{\mathrm{NEDE}} \to \Delta N_{\mathrm{IR}}$ alleviating the Hubble tension. The first step is related to the phase transition, and the second is related to the dark Higgs becoming nonrelativistic. This setup predicts further signatures, including a stochastic gravitational wave background and features in the matter power spectrum that can be searched for with future pulsar timing and Lyman-α forest measurements.

I. INTRODUCTION

The Hubble tension has risen to become one of cosmology's most hotly debated problems [1] and persists despite increasing levels of scrutiny [2]. Assuming it is not due to still unaccounted for systematics in the measurements, a resolution of the Hubble tension will have to involve new physics, going beyond the Lambda Cold Dark Matter (ΛCDM) model, at relatively low (∼eV) energy scales, where it will affect the cosmic microwave background (CMB) and other precision probes of the evolution of the Universe [3,4]. This makes the possible scenarios for resolving the Hubble tension very constrained and also very testable.

One of the earliest and simplest proposed solutions to the Hubble tension is the existence of a hypothetical fluid of strongly interacting dark radiation (SIDR) [5–7]. The SIDR solution has several incarnations. One is the so-called stepped model, where the SIDR fluid temporarily becomes nonrelativistic and then decays into a relativistic fluid again, creating a small step in the number of effective relativistic degrees of freedom, N_{eff} [8–11]. This mechanism allows for an ℓ-dependence in the CMB, with different impacts of the SIDR fluid on the high-ℓ and low-ℓ multipoles.

A common problem of the SIDR model, including the stepped models, is that they are ruled out by big bang nucleosynthesis (BBN) as solutions to the Hubble tension when taken at face value. Specifically, to address the Hubble tension, they require an initial value of the effective number of relativistic degrees of freedom, N_{eff}, which is too large to be compatible with BBN constraints [9]. This problem is usually circumvented by arguing that "something" could happen after BBN, creating the initially large N_{eff} required in the SIDR and the stepped models, but this something has not been included in the models in the literature so far at the detailed level (although for some initial suggestions, see Refs. [12–15] and Sec. II B below). Without further modification, SIDR and stepped models are therefore ruled out as solutions to the Hubble tension by BBN constraints.

*Contact author: mathias.garny@tum.de
†Contact author: florian.niedermann@su.se
‡Contact author: henrique.rubira@tum.de
§Contact author: sloth@sdu.dk

023531-1

In fact, we take the point of view that BBN physics cannot be separated from the solution to the Hubble tension when fitting the CMB. This is emphasized by the fact that the details of CMB and recombination physics depend on the helium fraction predicted by BBN. Therefore, the CMB and recombination physics are not independent from BBN physics.[1] The predictions of BBN are important for the full subsequent thermal evolution of the Universe. Therefore, a serious complete model solving the Hubble tension must also be required to be consistent with BBN constraints.

In this work, we show how, in terms of a dark sector described by a simple microphysical model, a first-order phase transition triggered by the temperature of the dark sector (named hot new early dark energy [hot NEDE] in Refs. [16,17]) provides the UV completion of the SIDR and stepped models, bringing them in agreement with the BBN constraints as solutions to the Hubble tension. In particular, we consider a standard Lagrangian described by an $SU(N)$ gauge symmetry and a massive dark Higgs field with quartic coupling as only ingredients, leading to spontaneous symmetry breaking $SU(N) \to SU(N-1)$. As pointed out by Witten [18], this setup features a strongly supercooled first-order phase transition *à la* Coleman-Weinberg [19] in the conformal limit where the effective scalar mass vanishes. In conclusion, when the latent heat of the false vacuum is converted into light species in the phase transition, the number of effective relativistic degrees of freedom, $N_{\rm eff}$, is suddenly increased.

If the hot NEDE phase transition occurs between the BBN and recombination epochs, i.e., roughly within the wide redshift range $10^5 \lesssim z_* < 10^9$, this explains how a relatively large $N_{\rm eff}$, as required in the SIDR and stepped models, can be made consistent with BBN constraints. The dark radiation component generated after the phase transition naturally gives rise to a sizeable change $\Delta N_{\rm eff} \sim \mathcal{O}(1)$. It is composed of massless $SU(N-1)$ gauge bosons as well as a light-dark Higgs boson, featuring self-interactions as assumed in SIDR models generated by the remaining non-Abelian $SU(N-1)$ gauge interactions for $N \geq 3$. In addition, a small mass of the dark Higgs is a characteristic feature of the Coleman-Weinberg mechanism. Thus, it turns nonrelativistic somewhat after the phase transition, leading to a further slight increase of $N_{\rm eff}$ in a second "step," and providing a natural realization of the stepped SIDR framework.

In Sec. II, we will review the NEDE framework and the SIDR models as solutions to the Hubble tension. In Sec. III, we explain our new dark sector model. In Sec. IV, we compare our model with cosmological datasets and discuss

how it can alleviate the Hubble tension. Then, in Sec. V, we discuss novel phenomenological signatures of the model, and finally we conclude and give pointers for future work in Sec. VI. The Appendixes contain further details on our results as well as equations used to describe the evolution after the phase transition.

II. BACKGROUND AND PRELIMINARIES

A. Comparison to cold NEDE

NEDE is a framework for addressing the Hubble tension in terms of a new phase of dark energy which decays in a fast-triggered phase transition before or around matter-radiation equality [20–22]. It is distinct from other early dark energy models, most notably axion-like EDE (axiEDE) [23] (for a review, see Ref. [24]) both in terms of its detailed phenomenology and field-theoretic realization.

Hot NEDE [16,17,25] is also different from the previously studied cold NEDE models [20,21], in which the phase transition is triggered by an ultralight axionlike (ULA) scalar field at zero dark sector temperature [26]. In particular, the cold NEDE fluid is usually assumed to have a constant equation of state $w \simeq 2/3$ after the phase transition as a phenomenological requirement for solving the Hubble tension. We note, however, that $N_{\rm eff}$ is the same in cold NEDE and in ΛCDM, making it trivially consistent with BBN constraints. In hot NEDE, there is no ULA, and the phase transition is instead triggered by the dark sector temperature corrections to the NEDE boson's effective potential. After the phase transition, the latent heat of the false vacuum goes into reheating the dark sector, creating a nontrivial change in $\Delta N_{\rm eff}$.

One of the main attraction points of hot NEDE as a solution to the Hubble tension is that it is a phase transition similar to other transitions such as the QCD and electroweak transitions that are already part of our understanding of the thermal history of the Universe. As we point out, the microscopic description of hot NEDE can be reminiscent of a dark version of the electroweak phase transition with a light Higgs. Besides, it could also be related to other open questions, such as the origin of neutrino masses [16,17]. However, while cold NEDE has been implemented into a Boltzmann code and studied rigorously in the past, a phenomenological test of hot NEDE has not yet been performed. In this paper, we will, for the first time, implement hot NEDE into a Boltzmann code and test it against data.

Previously, it was assumed that the phenomenology of hot NEDE from a CMB point of view would be very similar to cold NEDE. In this work, however, we point out that the phenomenology of hot and cold NEDE differs greatly. The fluctuations in the thermal trigger of hot NEDE are larger than in the scalar trigger of cold NEDE. This means that the hot NEDE model cannot resolve the Hubble tension by simply decaying into a semistiff fluid with the equation of

---

[1]Assuming a different value of $\Delta N_{\rm eff}$ at the time of BBN than around the recombination era would require manually setting the helium abundance at the CMB epoch to an assumed value. Instead, having a complete model allows one to consistently infer the helium abundance from BBN.

state $w \simeq 2/3$ around redshift $z_* = 5000$, as is typical in previously studied (N)EDE models, like cold NEDE. Instead, in hot NEDE, the phase transition must occur earlier (but after BBN) at a redshift $10^5 \lesssim z_* < z_{BBN} \sim 10^9$. After the phase transition, the NEDE boson and gauge fields will naturally behave like a SIDR fluid, mimicking the SIDR and stepped models around recombination yet with a natural explanation for the initial high N_{eff} created after BBN, and in this way UV completing the SIDR and stepped models as solutions to the Hubble tension.

B. Previous steps attempted

As exemplified by the initial suggestions mentioned above [12–15], increasing N_{eff} after BBN is not easy. One obvious idea would be to have an extra mass threshold leading to a second step in the stepped SIDR model, with both steps in N_{eff} happening after BBN. Another of the previously discussed possibilities is having some dark degrees of freedom which thermalize late through the neutrino sector after BBN. Let us quickly discuss both of these ideas for generating a sufficiently large N_{eff} after BBN, before we proceed to discuss in detail how a phase transition with a certain amount of supercooling between BBN and before recombination provides a conceptually simple mechanism.

As mentioned, one may wonder whether a "double step" scenario could reconcile the extra radiation needed to address the H_0 tension within the stepped SIDR model with BBN constraints.[2] This would be a scenario with a dark sector featuring one mass threshold to address H_0 and an earlier one after BBN to obtain a sufficient energy density in the dark sector. Assume real scalars, with $n_{IR} < n_{UV} < n_{BBN}$ degrees of freedom, where n_{UV} refers to the number of degrees of freedom in the period between the two steps, n_{BBN} before the two steps, and n_{IR} after them. The contribution to N_{eff} is then $\Delta N_{IR} = (n_{UV}/n_{IR})^{1/3} \Delta N_{UV}$ and $\Delta N_{UV} = (n_{BBN}/n_{UV})^{1/3} \Delta N_{BBN}$. Given BBN bounds $\Delta N_{eff} = -0.11 \pm 0.23$ [32] or $\Delta N_{eff} = -0.10 \pm 0.21$ [33], we require $\Delta N_{BBN} \lesssim 0.1$ in order not to introduce any tension with BBN. Assuming the dark sector was in thermal contact in the early Universe, the minimal contribution to ΔN_{eff} for a real scalar is 0.027 (e.g., Ref. [34]). This means we can have at most $n_{BBN} = 4$. Further assuming the minimal possible $n_{IR} = 1$ and $n_{UV} = 2$, this means we can have at most $\Delta N_{UV} = (4/2)^{1/3} 4 \times 0.027 \simeq 0.14$ and $\Delta N_{IR} = (2/1)^{1/3} \Delta N_{UV} \simeq 0.17$, which is too low to address the H_0 tension. To achieve the desired $\Delta N_{IR} \simeq 0.6$, one would, even in the most favorable case with $n_{IR} = 1$, need $n_{BBN} = (0.6/0.027)^{3/4} \simeq 10$ degrees of freedom during BBN, which would mean

$\Delta N_{BBN} \simeq 0.27$. Although not being completely excluded, this would arguably just trade the H_0 for a BBN tension.

A logical possibility for which the double step could work in principle is to assume that the dark sector was never in thermal equilibrium with the SM and populated with a lower temperature. While this by itself is a plausible possibility, enhancing the dark sector density sufficiently just due to mass threshold effects is still challenging in this scenario. Specifically, to have $\Delta N_{BBN} \lesssim 0.1$ but nevertheless achieve $\Delta N_{IR} \simeq 0.6$ via mass threshold effects for addressing the H_0 tension would require a large number of particles in the dark sector with $n_{BBN} \simeq (0.6/0.1)^3 n_{IR} \simeq 200 \, n_{IR} \geq 200$ degrees of freedom (where we assumed the minimal value $n_{IR} = 1$ in the last estimate) that all exhibit a mass threshold after BBN but sufficiently before recombination [15]. Having more degrees of freedom than contained in the entire Standard Model (SM) that undergo a nontrivial thermal evolution in the dark sector in the energy range between BBN and recombination is, however, a rather nonminimal proposal.

It has also been suggested that the constraints from BBN could be avoided if the dark sector temperature was effectively zero at the time of BBN and only created after BBN through thermalization of dark sector fermions with the SM neutrinos, which have decoupled at this point [15]. Since the SM neutrinos have decoupled from the SM, the thermalization with the dark sector does not by itself change N_{eff}, as it does not change the total energy density of the dark sector and SM neutrinos. However, if one or more of the self-interacting dark fermions subsequently undergo a mass threshold and annihilate into a much lighter force carrier, then that would lead to a second step as discussed above, but without affecting BBN if the dark fermions have a mass $100 \text{ eV} \lesssim m_{\nu_d} \lesssim 100 \text{ keV}$. In Ref. [15], it was argued that this allows for $\Delta N_{eff} = [(g_{rel,d}^{UV}/g_{rel,d}^{IR})^{1/3} - 1]N_{eq}$ where N_{eq} is the number of SM neutrinos equilibrating with the dark fermions, and $g_{rel,d}^{UV}$ and $g_{rel,d}^{IR}$ are the effective number of degrees of freedom before and after the mass threshold, respectively. To have $\Delta N_{eff} \approx 0.6$, as relevant for solving the Hubble tension, one would need four dark self-interacting fermions with masses $100 \text{ eV} \lesssim m_{\nu_d} \lesssim 100 \text{ keV}$ equilibrating with the SM neutrinos through a nonvanishing mixing angle $\theta > 10^{-13}$. However, it is plausible that the SIDR after the mass threshold consists of more than a single degree of freedom, making $g_{rel,d}^{IR} > 1$, and hence a very large dark sector equilibrating with the SM neutrinos after BBN is again quickly required.[3]

---

[2]An additional possibility, which we will not discuss here, is provided by nonrelativistic particles that decay after BBN [27–31].

[3]In addition, the proposed mixing of active neutrinos and a sterile neutrino with a self-interaction mediated by a light boson also suffers model-dependent constraints from stellar and supernova cooling [35,36].
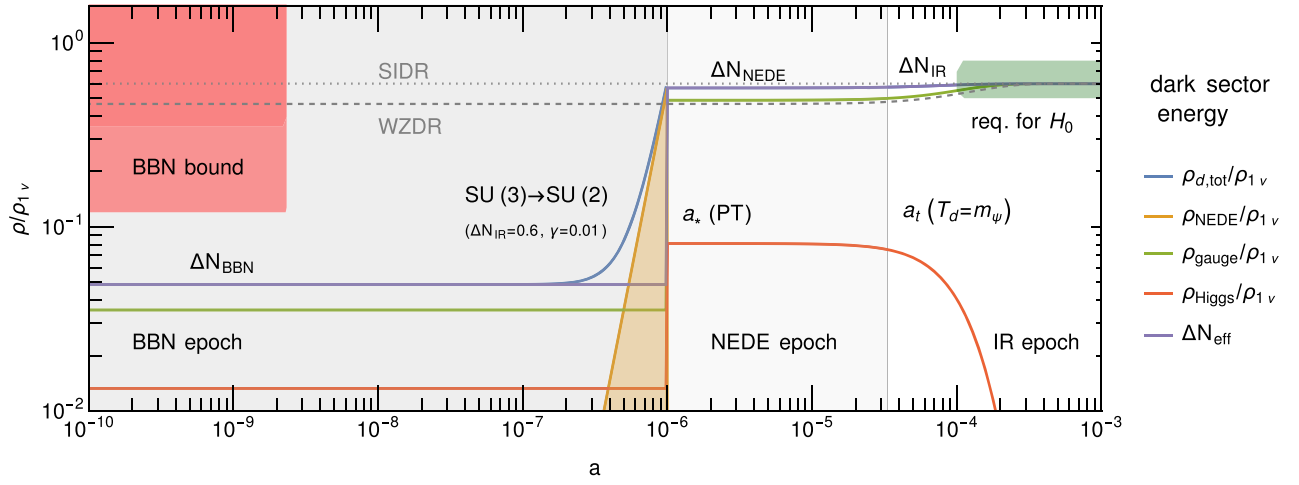
FIG. 1. Energy density of different dark sector components in units of $\rho_{1,\nu} \equiv \frac{7}{4}\frac{\pi^2}{30}(\frac{4}{11})^{4/3}T_{\text{vis}}^4$. The blue line depicts the evolution of the total dark sector energy density, composed of the dark radiation plasma formed by the gauge (green line) and Higgs (red line) bosons as well as the latent heat ρ_{NEDE} (orange line and area), that rises above the radiation fluid before the supercooled phase transition. The purple line depicts ΔN_{eff} before and after the phase transition at a_*; respectively, see (32) and (33). The red shaded area illustrates BBN constraints, and the green area illustrates values of ΔN_{eff} required for addressing the H_0 tension. For comparison, gray dotted and dashed lines show the SIDR model and its stepped version named WZDR [8] (see Sec. I).

While this remains a viable possibility, we will instead consider a simple new proposal, namely that both a significant dark sector temperature and a ΔN_{eff} are created by an energy injection into the dark sector from a super-cooled phase transition between BBN and recombination in the hot NEDE scenario. As we will see, all desired ingredients to realize this scenario naturally emerge from a dark sector described by a standard setup from the point of view of particle physics.

III. ORIGIN OF DARK SPECIES

Our dark sector model relies on a local $SU(N)$ gauge symmetry, which is spontaneously broken to $SU(N-1)$ by a scalar field undergoing a first-order phase transition. Our main focus centers on the evolution of this sector's contribution to the effective number of relativistic degrees of freedom, ΔN_{eff}, before and after the phase transition, featuring an increase related to the latent heat (the first step). Later, yet less importantly, the scalar field driving the phase transition becomes nonrelativistic, leading to a second change in N_{eff} (the second step), in a process similar to the step described in Ref. [8]. The evolution of ΔN_{eff} as well as the various dark sector energy densities are shown in Fig. 1 for a typical setup, and all relevant parameters are summarized in Table I. We discuss how this conceptually simple and well-known setup naturally generates a consistent cosmological evolution throughout BBN, recombination, and all the way until the present era, alleviating the Hubble tension while retaining the success of BBN.

We introduce the model's Lagrangian in Sec. III A. Then, we derive the parameter regime corresponding to a

supercooled phase transition in Sec. III B. The latent heat deposited in the dark sector leads to a very quick reheating as discussed in Sec. III C This is followed by a review of the second step in Sec. III D. Finally, in Sec. III E, we describe the perturbations in the plasma.

A. Model

We consider a dark sector featuring a gauge symmetry $SU(N)$ with gauge coupling g and a complex scalar field Ψ described by the standard Lagrangian

$$\mathcal{L} = |D\Psi|^2 - V_{\text{cl}}(|\Psi|^2) - \frac{1}{2}\text{tr}F_{\mu\nu}F^{\mu\nu}, \qquad (1)$$

where D is the gauge covariant derivative, with $D^\mu\Psi = \partial^\mu\Psi - igA_a^\mu\tau^a\Psi$ and also with generators satisfying $[\tau^a, \tau^b] = if^{abc}\tau^c$ with structure constants f^{abc}. Here $F^{\mu\nu} = ig^{-1}[D^\mu, D^\nu]$ is the field strength tensor. The dark Higgs field Ψ transforms in the fundamental representation of $SU(N)$, and we refer to it as the NEDE scalar field. Its zero temperature tree-level potential is given by

$$V_{\text{cl}}(|\Psi|^2) = -\mu^2|\Psi|^2 + \lambda|\Psi|^4 + V_0, \qquad (2)$$

where μ^2 is the field's (tachyonic) mass parameter and λ is its self-coupling. V_0 is an additive constant, which is chosen such that the potential energy is zero in the true vacuum.

As we will discuss in detail later, the gauge field induces thermal corrections that will lead to a first-order phase transition at a redshift $z_* \equiv 1/a_* - 1$ corresponding to a

TABLE I. Summary of the fundamental and phenomenological model parameters. The reference values correspond to a typical hot NEDE cosmology (also depicted in Fig 1). Once μ_{eff}, v, g, and N, alongside an initial condition for ΔN_{BBN}, are fixed, all other parameters can be derived.

Parameter	Eq.	Reference model	Description
g	(1)	0.05	Gauge coupling with lower bound [see (24)] $g \gtrsim 0.01$.
N	(1)	3	Gauge group breaking pattern: $SU(N) \to SU(N-1)$.
v	(5)	1.4×10^4 eV	NEDE field vacuum expectation value (vev) arising from dimensional transmutation.
μ_{eff}	(5)	1.1 eV	Renormalized mass parameter of NEDE field, describes small soft breaking of classical conformal symmetry for $\mu_{\text{eff}} \ll g^2 v$, provides graceful exit from supercooling.
$m_A \equiv gv/2$	$\cdots$	3.5×10^2 eV	Gauge boson mass scale after symmetry breaking.
$m_\psi \sim g^2 v$	(7)	4.4 eV	Dark Higgs mass.
$\Delta V_* \sim g^4 v^4$	(14)	$(127 \text{ eV})^4$	Latent heat released during the phase transition.
$\lambda \sim g^4$	(2)	5.0×10^{-8}	Tree-level self-coupling of the NEDE field.
$\gamma \sim \mu_{\text{eff}}^2/(g^4 v^2)$	(12)	0.01	Supercooling parameter, strong supercooling for $\gamma \ll 1$.
$T_c \sim gv$	(10)	1.2×10^2 eV	Dark sector temperature with two degenerate vacua.
$T_d^* \sim \sqrt{\gamma} gv$	(18)	39.2 eV	Dark sector temperature when percolation condition is met ($T_d^* \simeq T_b$ in the supercooling regime).
$T_b \sim \sqrt{\gamma} gv$	(11)	39.1 eV	Dark sector temperature below which thermal barrier vanishes.
$T_d^{*,\text{after}} \sim \Delta V_*^{1/4}$	(26)	1.0×10^2 eV	Dark sector temperature after the phase transition.
T_{vis}^*	(18)	2.4×10^2 eV	Visible sector temperature during the phase transition.
H_*/β	(20)	2.9×10^{-6}	Percolation time scale.
α	$\cdots$	0.076	Strength of phase transition, $\alpha \equiv \Delta V/(\rho_{\text{rad,vis}}^* + \rho_{\text{rad,d}}^*)$.
z_*	$\cdots$	10^6	Redshift of the NEDE phase transition (first step) with possible range: $[10^5, 10^9]$.
$z_t \sim g z_*$	(31)	4.2×10^4	Redshift when the dark Higgs becomes non-relativistic, i.e. for which $m_\psi = T_d$ (second step) with $z_t < z_*$.
f_{NEDE}	(14)	0.071	Fraction of latent heat at redshift z_*, setting the size of the first step. Note that $f_{\text{NEDE}} = \alpha/(1 + \alpha)$.
r_g	(B9)	1/6	Size of the second step.
ΔN_{BBN}	(19)	0.039	Contribution to ΔN_{eff} before the NEDE phase transition, applicable during BBN.
ΔN_{NEDE}	(27)	0.57	Contribution to ΔN_{eff} after the NEDE phase transition.
ΔN_{IR}	(29)	0.6	Contribution to ΔN_{eff} after the second step.

dark sector temperature T_d^*.[4] As the symmetry breaking from $SU(N) \to SU(N-1)$ occurs, the NEDE field picks up a vacuum expectation value v. We parametrize the corresponding breaking pattern through

$$\Psi = e^{2i\pi^a \tau^a/v} \begin{pmatrix} 0 \\ \cdots \\ \frac{v}{\sqrt{2}} + \frac{h_\psi}{\sqrt{2}} \end{pmatrix}, \qquad (3)$$

---

[4]Here and henceforth, an asterisk is used as a shorthand for evaluation at the moment of the phase transition. If a quantity is discontinuous, we refer to its value *before* the transition; e.g., T_d^* is the (dark sector) temperature right before the phase transition (also sometimes denoted as T_n in the literature).

where h_ψ is the physical Higgs mode of the NEDE field after the phase transition and π^a are the Goldstone fields associated with the $2N - 1$ broken generators τ^a that are absorbed by the gauge bosons acquiring mass. Let us consider the example of $SU(3) \to SU(2)$ in more detail. After the breaking, there are three massless states, $m_{A_1} = m_{A_2} = m_{A_3} = 0$, corresponding to $n_{A_{1-3}} = 6$ degrees of freedom. The remaining five gauge bosons are massive. Explicitly, $m_{A_4} = m_{A_5} = m_{A_6} = m_{A_7} = \frac{gv}{2}$ with $n_{A_{4-7}} = 4 \times 3 = 12$, and $m_{A_8} = \frac{gv}{\sqrt{3}}$ with $n_{A_8} = 3$. The physical NEDE mode develops a vacuum mass m_ψ, of order $g^2 v$; see (7) below. The numbers of massless and massive degrees of freedom in both phases are also summarized in Table II for general N.

TABLE II. Degrees of freedom (d.o.f.) in the dark sector. The first row shows the relativistic d.o.f. $g_{\mathrm{rel},d}$ before ($z > z_*$) and after ($z < z_*$) the $SU(N) \to SU(N-1)$ phase transition, further discriminating the regime where the Higgs is relativistic ($z > z_t$) or nonrelativistic ($z < z_t$). The lower rows show the d.o.f. of each species.

No. of d.o.f.	$z > z_*$ (BBN)	$z_* > z > z_t$ (NEDE)	$z < z_t$ (IR)
$g_{\mathrm{rel},d}$	$2(N^2 + N - 1)$	$2(N-1)^2 - 1$	$2(N-1)^2 - 2$
Massless gauge bosons	$2(N^2 - 1)$	$2((N-1)^2 - 1)$	
Massive gauge bosons	0	$n_A \equiv 3(N^2 - (N-1)^2) = 3(2N-1)$	
Higgs bosons	$2N$	1	

B. Phase transition

We now describe the physics of the thermal phase transition at $z = z_*$, focusing on the regime of a supercooled first-order phase transition, that permits a sizeable step in ΔN_{eff}. This occurs in the limit for which the dark Higgs mass is light compared to the gauge boson masses [18][5]

$$m_A \gg T_d^*, m_\psi, \qquad (4)$$

being realized for $\lambda \sim g^4$. Adopting this power counting, the phase transition can be described by the one-loop approximation of the effective potential taking gauge boson loops into account. It can be written as

$$V(\psi; T_d) = V_0 - \frac{\mu_{\mathrm{eff}}^2}{2} \psi^2 \left(1 - \frac{\psi^2}{2v^2}\right) + B\psi^4 \left(\ln \frac{\psi^2}{v^2} - \frac{1}{2}\right)$$
$$+ \Delta V_{\mathrm{thermal}}(\psi; T_d), \qquad (5)$$

where $\psi \equiv \sqrt{2}|\Psi|$ denotes the field value. Let us review the various contributions in turn. First of all, note that we traded the tree-level parameters μ^2 and λ in (1) by[6] μ_{eff}^2 and v^2 such that $\mu_{\mathrm{eff}}^2 = 0$ corresponds to the classically conformal limit for which symmetry breaking famously occurs purely due to the radiative correction proportional to B [see (6)] and the scale v is generated by dimensional transmutation as pointed out by Coleman and Weinberg [19]. For generality, we allow for nonzero (but potentially small) values μ_{eff}^2 of order up to $v^2 g^4$, consistent with the power counting $\lambda \sim g^4$, which can be seen as a technically natural "soft" breaking of conformal symmetry. The parameter B is

$$B = \frac{c_1 n_A}{64\pi^2} \left(\frac{g}{2}\right)^4, \qquad (6)$$

where n_A is the number of gauge bosons acquiring mass (see Table II) and c_1 is a constant of order unity ($c_1 = 52/45$ for $N = 3$).[7] In this parametrization, the minimum of the vacuum potential in the first line of (5) occurs at $\psi = v$, and the constant V_0 ensures $V(v; 0) = 0$.

A well-known case featuring very strong supercooling, discussed by Witten [18] (see also Ref. [45]), is the conformal limit $\mu_{\mathrm{eff}} = 0$. As we will see, a small nonzero μ_{eff} [related to the supercooling parameter γ defined in (12) below] provides a graceful exit mechanism allowing for a controlled amount of supercooling and preventing the latent heat from dominating the total energy budget [16,41]. As in the purely conformal limit, the dark Higgs is parametrically lighter than the gauge boson masses,

$$m_\psi^2 = \frac{d^2 V}{d\psi^2}(v; 0) = 2\mu_{\mathrm{eff}}^2 + 8Bv^2 \ll m_A^2 \sim g^2 v^2. \quad (7)$$

The second line in (5) denotes the thermal correction given by [46–48]

$$\Delta V_{\mathrm{thermal}}(\psi; T_d) = \frac{1}{2\pi^2} \sum_i n_i T_d^4 J_B(m_i^2(\psi)/T_d^2), \quad (8)$$

where $J_B(a^2) = \int_0^\infty dp\, p^2 \ln(1 - e^{-\sqrt{p^2 + a^2}})$ and the sum runs over all species with field-dependent masses m_i and n_i degrees of freedom. The parametrization $J_B(a^2) \equiv 2\pi^2 K(a)e^{-a}$ from Ref. [16] makes the Boltzmann suppression for $a \gg 1$ explicit, while $K(a)e^{-a} \simeq -\pi^2/90 + a^2/24 - a^3/(12\pi) + \cdots$ in the opposite limit. In the supercooled regime $\lambda \sim g^4$, it is sufficient to include only the gauge bosons with masses $m_A \sim gv$ in the sum and omit Debye corrections known as ring resummation [48]; see Refs. [43,49] for further discussion. The leading ψ-dependent thermal correction for $T_d \gg g\psi$ is

$$\Delta V_{\mathrm{thermal}}(\psi; T_d) \to \frac{1}{24} c_0 n_A g^2 T^2 \psi^2, \qquad (9)$$

where as before n_A is the number of gauge bosons acquiring mass (see Table II) and c_0 is another model-dependent constant of order unity ($c_0 = 4/15$ for $N = 3$). In the opposite limit $T_d \ll g\psi$, the thermal correction is exponentially suppressed.

The thermal correction restores the $SU(N)$ symmetry at high temperatures, while a second minimum at nonzero

---

[5]See also Refs. [16,17] for more details in the context of hot NEDE and, e.g., Refs. [37–44] for a discussion of supercooling in other scenarios.

[6]The relation to (1) is $\mu^2 = \mu_{\mathrm{eff}}^2 + 4Bv^2 = \lambda v^2$.

[7]$c_1 = \frac{3}{n_A} 16 \sum_a m_{A_a}^4(\psi)/(g\psi)^4$, and $c_0 = \frac{3}{n_A} \sum_a m_{A_a}^2(\psi)/(g\psi)^2$.

$\psi = v_\psi(T)$ develops and becomes degenerate with the one at $\psi = 0$ at the critical temperature T_c. For $\mu_{\text{eff}}^2 \lesssim v^2 g^4$, one has[8]

$$T_c \sim gv, \tag{10}$$

and $v_\psi(T_c) \sim v_\psi(0) = v$. The two minima are separated by a barrier, such that the phase transition is of first order in the regime we consider. The transition temperature T_d^* at which bubbles of the true vacuum are nucleated is significantly below the critical temperature in the supercooled regime, $T_d^* \ll T_c$. In the conformal case $\mu_{\text{eff}} = 0$, the barrier becomes small but does not vanish (unless the temperature vanishes exactly), leading to potentially very strong supercooling; see, e.g., Refs. [41–43]. For nonzero μ_{eff}, the barrier vanishes at a finite temperature, given approximately by the temperature T_b for which $d^2V/d\psi^2(0; T_b)$ changes sign,

$$T_b^2 = \frac{12\mu_{\text{eff}}^2}{c_0 n_A g^2} = \frac{\gamma}{\pi} g^2 v^2, \tag{11}$$

where we introduced the supercooling parameter [16]

$$\gamma \equiv \frac{12\pi\mu_{\text{eff}}^2}{c_0 n_A v^2 g^4}. \tag{12}$$

The conformal limit of radiative symmetry breaking *à la* Coleman-Weinberg corresponds to $\gamma \to 0$, while supercooling occurs as long as $\gamma \lesssim \mathcal{O}(1)$. The parameter γ can take in principle any value in this range, being arguably technically natural since classical conformal symmetry is restored for $\gamma = 0$. Its size controls the amount of supercooling. To determine the temperature at which the phase transition occurs, we can discriminate two regimes. For this, it is useful to consider the temperature $T_d^*|_{\text{CW}}$ for which tunneling would occur with unit probability in a Hubble volume and time in the Coleman-Weinberg case $\gamma = 0$. The first (rather extreme) possibility is that γ is so small that $T_b < T_d^*|_{\text{CW}}$, and the transition happens essentially at the same time as it would occur for $\gamma = 0$. This is the case for $\gamma \ll (T_d^*|_{\text{CW}})^2/(gv)^2$. The second case, that we consider in the following, occurs if $\gamma \gtrsim (T_d^*|_{\text{CW}})^2/(gv)^2$, such that $T_b > T_d^*|_{\text{CW}}$. In this case, the μ_{eff}^2 contribution to the effective potential makes the barrier vanish already before the field would have tunneled in the Coleman-Weinberg case. Then, the transition occurs very shortly before the barrier vanishes at temperature T_b, i.e.,

---

[8]A more precise value can be easily obtained using the parametrization of $K(a)$ in Ref. [16] (see also Table I for a numerical example).

$$T_d^* \simeq T_b = \sqrt{\frac{\gamma}{\pi}} gv \sim \sqrt{\gamma} T_c, \tag{13}$$

applicable for $(T_d^*|_{\text{CW}})^2/(gv)^2 \lesssim \gamma \lesssim 1$, which we assume in the following. The parametric dependence for small g can be estimated as [18] $T_d^*|_{\text{CW}} = v \exp(-\mathcal{O}(1)/g^3)$ when using the percolation condition $S_3^*/T_d^* \simeq 250$ (taken from Ref. [16]; see also Ref. [42]). For $g \lesssim 1$, as assumed in this work, we can thus safely neglect the effect of a nonvanishing $T_d^*|_{\text{CW}}$.

For our purpose, we are interested in the latent heat

$$\Delta V_* = V(\psi = v_\psi(T_d^*); T_d^*) - V(\psi = 0; T_d^*) \tag{14}$$

released in the phase transition. For $\gamma \lesssim 1$, one can estimate the latent heat by the potential energy difference between the two phases in the limit $T = 0$,

$$\begin{aligned}
\Delta V_* &\simeq V(v; 0) - V(0; 0) = \frac{1}{2} B v^4 + \frac{1}{4}\mu_{\text{eff}}^2 v^2 \\
&= g^4 v^4 \frac{(3c_1 + 128\pi c_0\gamma)n_A}{6144\pi^2} = T_b^4 \frac{(3c_1 + 128\pi c_0\gamma)n_A}{6144\gamma^2},
\end{aligned} \tag{15}$$

where we used (11), (12).

The relevance of having a strongly supercooled phase transition becomes clear when considering the contribution to N_{eff} before and after the phase transition. In terms of the temperature ratio $\xi = T_d/T_{\text{vis}}$, it is given by (assuming a purely bosonic field content)

$$\Delta N_{\text{eff}} = \frac{4}{7}\left(\frac{11}{4}\right)^{4/3} g_{\text{rel,d}} \xi^4, \tag{16}$$

where $g_{\text{rel,d}}$ ($g_{\text{rel,vis}}$) denotes the number of relativistic degrees of freedom in the dark (visible) sector. We further introduce the maximal fraction of vacuum energy stored in the scalar field just before the phase transition, dubbed "new early dark energy," as

$$f_{\text{NEDE}} = \Delta V_*/\rho_{\text{tot}}(T_d^*), \tag{17}$$

where $\rho_{\text{tot}}(T_d^*) \simeq \pi^2 g_{\text{rel,vis}}^* T_d^{*4}/(30\xi_*^4) + \Delta V_*$ (when neglecting the small contribution of the dark sector radiation plasma before the transition). This allows us to express ξ_*, i.e., the relative dark sector temperature right before the phase transition, in terms of f_{NEDE} as[9]

---

[9]When combining with (15), this reproduces the result in [16] for $n_A = 3$ and $c_0 = 1$ when we neglect one-loop corrections (corresponding to the formal limit $c_1 \to 0$). This tree-level approach is valid in the mildly supercooled regime with $1 \gtrsim \gamma \gtrsim 0.03$ (for $N = 3$).

$$\xi_*^4 \simeq g_{\mathrm{rel,vis}}^* \frac{\pi^2}{30} \frac{f_{\mathrm{NEDE}}}{1 - f_{\mathrm{NEDE}}} \frac{(T_d^*)^4}{\Delta V_*}. \tag{18}$$

Using the result (15) for the latent heat, and $T_b \simeq T_d^*$ in the strongly supercooled regime, we obtain a (small) contribution to N_{eff} *before* the phase transition

$$\Delta N_{\mathrm{BBN}} \simeq \frac{32}{35} \left(\frac{11}{4}\right)^{4/3} \frac{128\pi^2\gamma^2 g_{\mathrm{rel,d}}^* g_{\mathrm{rel,vis}}^*}{(3c_1 + 128\pi c_0\gamma)n_A} \frac{f_{\mathrm{NEDE}}}{1 - f_{\mathrm{NEDE}}}$$
$$\simeq 0.055 \frac{\frac{N^2+N-1}{2N-1}}{11/5} \left(\frac{\gamma}{0.01}\right)^2 \frac{52/45}{c_1} \frac{f_{\mathrm{NEDE}}}{0.08}, \tag{19}$$

where in the second line we used $g_{\mathrm{rel,vis}}^* = 3.38$, $g_{\mathrm{rel,d}}^* = 2N^2 + 2N - 2$, $n_A = 3(2N-1)$ (see Table II) and assumed $\gamma, f_{\mathrm{NEDE}} \ll 1$. From this, it is clear that if γ is sufficiently small, i.e., we are in the strongly supercooled regime, ΔN_{eff} can be made compatible with BBN. As a reference value for $N = 3$, we can satisfy the BBN bound $\Delta N_{\mathrm{BBN}} \lesssim 0.1$ for $\gamma\sqrt{f_{\mathrm{NEDE}}} \lesssim 0.004$ corresponding to $\xi_* \lesssim 0.21$. For our data fit, we will set $\xi_* = 0.1$, which allows us to satisfy the BBN bound for $N < 15$. As we will argue in detail in the next section, this subdominant dark radiation fluid, through its adiabatic perturbations δ_{DR}, sets the initial conditions for the perturbations, δ_{NEDE} and θ_{NEDE}, in the dark sector plasma after the phase transition. We highlight that the precise value of the background parameter ξ_* does not have any impact on the cosmological observables considered here as the corresponding energy density is suppressed by $(\xi_*)^4$.

C. Dark sector reheating

Another central point is the latent heat injection and thermalization of the dark sector after the phase transition.[10] A first-order phase transition leads to the nucleation of vacuum bubbles that separate the false (symmetric) from the true (broken) vacuum. As they expand, more and more space is converted to the true vacuum. Since we are considering strong supercooling, we expect that the latent heat released during this percolation phase is partially stored as kinetic and gradient energy in the bubble walls and partially in coherent scalar field oscillations. Notice that whether supercooling leads to a terminal bubble wall velocity or runaway bubbles demands further analysis, depending on the interaction with the plasma [50–54]. The coupling with the plasma induces sound waves [55–61] that can reheat the dark sector via other channels (e.g., via heat dissipation in turbulence [62–64]). As these bubbles start to collide, they break up into smaller fragments and form a field condensate of small-scale anisotropic stress. The

corresponding length scale is conventionally denoted in the gravitational wave literature as [65] β^{-1}, where $\beta \simeq \dot{\Gamma}/\Gamma$ quantifies the relative change in the transition rate Γ.[11] In the supercooled regime, it is given by Ref. [16] (see also Ref. [41]),

$$\beta^{-1} \sim 10^{-2} n_A^{1/3} g^2 H(t_*)^{-1} \ll H(t_*)^{-1}. \tag{20}$$

Given a small enough gauge coupling, it is indeed much smaller than cosmological scales set by $H(t_*)^{-1}$. For a more complete description of the gravitational wave phenomenology, see Sec. V A.

Depending on the microphysics, there are different possibilities as to how this system can evolve further. The massless gauge bosons offer a channel at one-loop level for the (nonthermal) scalar particles residing in the bubble wall condensate and coherent field oscillations to decay through triangle diagrams into pairs of massless $SU(N-1)$ gauge bosons, e.g., for $SU(2)$ $\psi \to A_{1-3} + A_{1-3}$.[12] This is similar to the $h \to \gamma\gamma$ process of the Standard Model. To be precise, we have [66]

$$\Gamma_{\psi \to AA}^{(\mathrm{cm})} = g^4 \frac{m_\psi^3}{v^2} \left(\frac{F}{16\pi^2}\right)^2 \frac{1}{2\pi}, \tag{21}$$

where F depends on the particle content running in the loop. In our case, where $m_A \gg m_\psi$, we can approximate it as a constant $F = \mathcal{O}(1)$. Setting $N = 3$ and employing (12), (11), and (7), we derive

$$\Gamma_{\psi \to AA}^{(\mathrm{cm})} \simeq \frac{F^2 g^9 T_d^*}{196608\sqrt{6}\pi^{15/2}} \frac{(13 + 64\pi\gamma)^{3/2}}{\sqrt{\gamma}}. \tag{22}$$

At the same time, we have

$$H_* = \frac{\pi}{\sqrt{90}} \frac{\sqrt{g_{\mathrm{rel,vis}}^*}}{\sqrt{1 - f_{\mathrm{NEDE}}}} \frac{T_{\mathrm{vis}*}^2}{M_{\mathrm{pl}}}. \tag{23}$$

Combining (22) and (23), we obtain the final estimate

$$\frac{\Gamma_{\psi \to AA}^{(\mathrm{cm})}}{H_*} = \mathcal{O}(1) \times \frac{g^9 f_{\mathrm{NEDE}}^{1/4}}{1 + z_*} 10^{24}, \tag{24}$$

---

[10]We refer to this process in analogy to the end of inflation as a "reheating". Note, however, that here, in the present work, we assume dark matter is not created in that process and considered to be cold.

[11]To be specific, if the time dependence of Γ is approximated as a linear exponential, the parameter β corresponds to the inverse duration of the phase transition. For a supercooled transition where the bubble walls quickly approach the speed of light, β^{-1}, therefore, corresponds to the typical bubble size at the time of collision.

[12]See Ref. [16] for two more possibilities, dubbed scenario A and B. One in which the NEDE boson is stable is expected to inhibit the decay and disintegration of the bubble wall condensate. Another one, which shares similarities with the scenario discussed here, has the bubble wall condensate decay into a stable massive particle that makes a contribution to dark matter.

where we used $T_{\mathrm{vis}*} \simeq 2.3 \times 10^{-4}(1 + z_*)$ eV alongside (18) and (15) and assumed $f_{\mathrm{NEDE}}, \gamma \ll 1$. Substituting the typical value $f_{\mathrm{NEDE}} = 0.08$, while demanding a post-BBN phase transition with $z_* < 10^8$, a sufficient condition for an efficient decay with $\Gamma_{\psi \to AA}^{(\mathrm{cm})} \gg H_*$ is $g \gtrsim 0.02$. We note that this calculation assumes that the ψ bosons are at rest at the time of decay, which will only be true right after the bubble nucleation. Also, it neglects bosonic enhancement effects, which might become sizeable. However, we do not expect these effects to significantly tighten the bound on g (after all, it is softened by the ninth root).

While the massless gauge bosons are being populated, they start to thermalize through their self-interactions, $A_{1-3} + A_{1-3} \to A_{1-3} + A_{1-3}$. Their interaction rate is $\Gamma_{\mathrm{therm}} = \langle \sigma v \rangle n_h$, where $\langle \sigma v \rangle$ is the velocity-averaged cross section. Here, we can employ the much cruder estimate $\Gamma \sim g^4 T_d = g^4 \xi_*^{\mathrm{after}} T_{\mathrm{vis}*}$ relying on a (partial) thermalization. With $\xi_*^{\mathrm{after}} \sim 0.5$, we find

$$\frac{\Gamma_{\mathrm{therm}}}{H_*} \sim \frac{g^4}{1 + z_*} 10^{31}, \tag{25}$$

which, even in the least favorable case with $z_* \sim 10^9$ and $g \sim 0.01$, ensures an extremely fast thermalization. This also applies to similar number-changing $2 \to 3$ or in general $n \to m$ processes involving the massless gauge bosons, that establish complete chemical and kinetic equilibrium with vanishing chemical potential and are parametrically similarly efficient as $2 \to 2$ processes in a non-Abelian plasma [67–69]. Once their temperature has reheated above m_ψ, the gauge bosons also populate and equilibrate the ψ bosons through the (inverse) decay process $A_{1-3} + A_{1-3} \leftrightarrow \psi$.

We have therefore established that both the percolation scale β as well as the decay and thermalization scales, $\Gamma_{\psi \to AA}^{(\mathrm{cm})}$ and Γ_{therm}, are large compared to H_*. In the following, we will thus treat the phase transition and subsequent reheating as an instantaneous process on cosmological timescales. As we will see, this simplifies the description of the evolution of both the background fluid and its perturbations.

After the reheating is completed, we can equate the dark sector radiation fluid with the latent heat ΔV_* (neglecting the small contribution from the preexisting thermal fluid that triggered the phase transition). An analog calculation to the one above the one described above then yields the contribution to N_{eff} *after* the phase transition. To be specific, we find

$$(\xi^{*,\mathrm{after}})^4 = \frac{g^*_{\mathrm{rel,vis}}}{g^{\mathrm{after}}_{\mathrm{rel,d}}} \frac{f_{\mathrm{NEDE}}}{1 - f_{\mathrm{NEDE}}}, \tag{26}$$

with $g^{\mathrm{after}}_{\mathrm{rel,d}} = 2[(N - 1)^2 - 1] + 1$ (see Table II). Using (16), this translates into

$$\Delta N_{\mathrm{NEDE}} \simeq \frac{4}{7} \left(\frac{11}{4} \right)^{4/3} g^*_{\mathrm{rel,vis}} \frac{f_{\mathrm{NEDE}}}{1 - f_{\mathrm{NEDE}}}$$

$$\simeq 7.4 \frac{f_{\mathrm{NEDE}}}{1 - f_{\mathrm{NEDE}}}. \tag{27}$$

We note that ΔN_{NEDE} should be identified with N_{UV} as used in the literature on the step model (see, for example, Ref. [8]). This shows that we can achieve ΔN_{NEDE} of order unity for $f_{\mathrm{NEDE}} \simeq 12\%$ (for $N = 3$, this corresponds to $\xi \simeq 0.5$). With the definitions in (27) and (19), we can summarize this *first step* as

$$\Delta N_{\mathrm{BBN}} \to \Delta N_{\mathrm{NEDE}} = \frac{5(3c_1 + 128c_0 \pi \gamma)n_A}{1024\pi^2 g^*_{\mathrm{rel,d}} \gamma^2} \Delta N_{\mathrm{BBN}}. \tag{28}$$

Therefore, a strongly supercooled phase transition with $\gamma \ll 1$ offers an efficient mechanism to heat the dark sector after BBN and introduce a sharp step in ΔN_{eff}.

D. Second step

After the phase transition, we have a two-component fluid, with the light dark Higgs bosons and the massless gauge bosons being in thermal and chemical equilibrium. However, when the NEDE bosons become nonrelativistic, their production channel becomes Boltzmann suppressed, and they decay into the massless gauge bosons, thereby depositing their entropy in the radiation fluid. Microscopically, this happens again through the triangle diagram $\psi \to AA$, and we can use (24) evaluated at redshift $z_t < z_*$ (up to an order unity factor accounting for the velocity distribution) to argue that the decay process is efficient, and thus this process can be described assuming thermal equilibrium, implying in particular entropy conservation, similarly as for $e^+ e^-$ annihilation in the visible sector. As a result, the previous contribution to N_{eff} increases further,

$$\Delta N_{\mathrm{NEDE}} \to \Delta N_{\mathrm{IR}} = \Delta N_{\mathrm{NEDE}}(1 + r_g)^{1/3}, \tag{29}$$

with r_g the relative change in the number of relativistic degrees of freedom. This second step has been studied extensively as a solution to the Hubble tension in the literature [8,9], and we review its derivation in Appendix B. For our model, we find $r_g^{-1} = 2N(N - 2) \geq 6$, which translates to a small step of less than 5.3%. We can constrain the redshift z_t of the second step, which is defined implicitly through $T_d(z_t) = m_\psi$. From the definition in (7) and (15), we derive[13]

---

[13]As noted before, a light Higgs state is one of the characteristics of a supercooled phase transition [18,19,39,40].

$$\frac{m_\psi^4}{\Delta V_*} = \frac{g^4 n_A (3c_1 + 64 c_0 \pi \gamma)^2}{24 \pi^2 (3c_1 + 128 c_0 \pi \gamma)}. \tag{30}$$

Together with the conditions $(1+z_t)/(1+z_*) = m_\psi / T_d^{*,\text{after}}$ and $\Delta V_* \simeq \frac{\pi^2}{30} g_{\text{rel,d}} (T_d^{*,\text{after}})^4$, this implies

$$\frac{1+z_t}{1+z_*} \simeq g \left(\frac{c_1 g_{\text{rel,d}}^{\text{after}} n_A}{240} \right)^{1/4}, \tag{31}$$

where we assumed $\gamma \ll 1$. As an explicit example, in the case of $N = 3$, we find that $(1+z_t)/(1+z_*) \simeq 0.84 g \gtrsim 0.02$, where we used our reheating bound $g \gtrsim 0.02$. As a result, the second step is constraint to occur within a few e-folds after the first step. This bound becomes even tighter for $N > 3$. However, in this case, $r_g \to 0$, and as a consequence the second step disappears in the large-N limit, see Fig. 2, such that the value of z_t does not play a role in that case. We anticipate that the second step has minor impact in the analysis, being not favored as a solution to H_0 (see Appendix A). This second step is therefore more an extra feature of our model then a necessary point to address the Hubble tension.

The entire two-step sequence, $\Delta N_{\text{BBN}} \to \Delta N_{\text{NEDE}} \to \Delta N_{\text{IR}}$, is depicted in Fig. 1 as the purple line. We stress that the first and second steps are physically distinct. While the thermally induced phase transition is first order and thus involves a discontinuous change in the fluid's entropy, the second step is a continuous process for which the entropy remains constant (see Fig. 2). The remaining evolution at background level is then simply that of a relativistic fluid.

To summarize, the dark sector fluid before the phase transition ($a < a_*$) is

$$\bar{\rho}_{\text{DR}}(a) + \Delta V_*, \tag{32}$$

where $\Delta V_* = \text{const}$ is the latent heat defined in (14) and $\bar{\rho}_{\text{DR}} = g_{\text{rel,d}} \frac{\pi^2}{30} T_d^4$ denotes the subdominant radiation fluid that triggers the phase transition. The bar notation indicates that we work at the background level. After the bubble percolation and subsequent thermalization have completed, we are left with a tightly coupled fluid composed of ψ particles and massless gauge bosons with an evolving equation of state parameter, giving rise to ($a > a_*$),

$$\bar{\rho}_{\text{NEDE}}(a) = [\Delta V_* + \bar{\rho}_{\text{DR}}(a_*)]$$
$$\times \exp \left[-3 \int_{a_*}^a d \ln \tilde{a} (1 + w(\tilde{a})) \right], \tag{33}$$

where $w(a)$ is defined in (B14). The time evolution for different contributions to the dark sector plasma is depicted in Fig. 1 as the orange (latent heat), red (Higgs), and green (massless gauge bosons) lines.

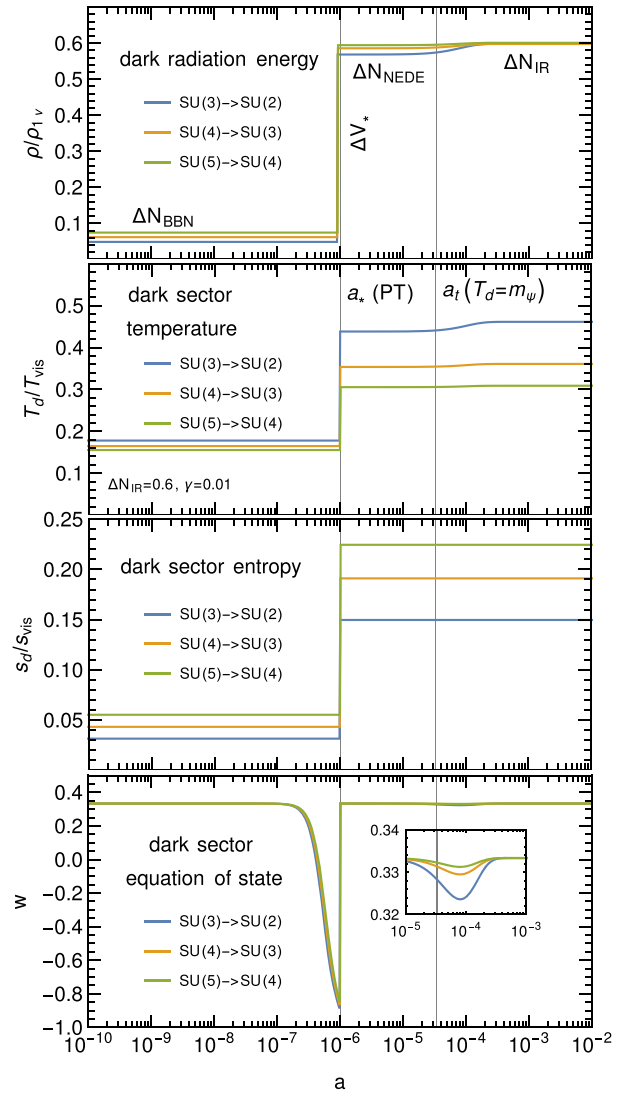Furthermore, a key assumption in our derivation is that the phase transition completes in much less than a Hubble

FIG. 2. Evolution of ΔN_{eff}, temperature ratio $\xi_d = T_d / T_{\text{vis}}$, entropy ratio s_d / s_{vis}, and equation of state $w = p_d / \rho_d$ for $SU(N) \to SU(N-1)$ with $N = 3, 4, 5$. All are discontinuous at the phase transition at a_* (first step), while only the entropy is conserved once the dark Higgs becomes nonrelativistic at a_t (second step). The second step disappears in the large-N limit. Note that for a growing number of degrees of freedom g_d (i.e., for $N = 3, 4, 5$) the temperature T_d decreases, while $s_d \propto g_d T_d^3$ increases with g_d for given $\Delta N_{\text{IR}} \propto g_d T_d^4$.

time. This allows us to describe it as an instantaneous process when implementing our model in a Boltzmann code. In the next section, we discuss how such an abrupt transition affects perturbations.

E. Perturbations

Next, we turn to perturbations in the dark sector radiation fluid. We will refer to them as dark sector acoustic oscillations (adapting the terminology used in the acoustic dark energy model [70]). Before the NEDE phase

transition, the subdominant dark radiation fluid carries adiabatic perturbations, while the NEDE vacuum acts like a (homogeneous) cosmological constant. After the phase transition, there are two main sources for perturbations in the radiation fluid. First, there are inhomogeneities related to the nucleation of bubbles of the broken symmetry phase. These perturbations are large and set by the density contrast between the bubble interior and exterior, explicitly $\delta_{\mathrm{NEDE}} \sim 1$ (as we can neglect the radiation plasma before the transition). However, they are only present on small scales $1/\beta$ set by the size of vacuum bubbles before they collide. In particular, for a phase transition that occurs much before recombination and g sufficiently small, these modes cannot be probed neither in the CMB nor in Large-scale structure (LSS) data.[14] Second, there are perturbations seeded by adiabatic perturbations of the (subdominant) radiation fluid that trigger the thermal phase transition. Let us stress that these perturbations are not a consequence of the stochastic character of the phase transition; instead, they are created because different spatial regions are slightly "ahead" or "behind" in time. In a coarse-grained approach valid on large scales, i.e., for spatial momenta $k \equiv |\mathbf{k}| \ll \beta^{-1}$, they can be derived by matching the cosmological perturbation theory across a surface of constant $\delta_{\mathrm{DR}}(\eta, \mathbf{k}) \equiv [\rho_{\mathrm{DR}}(\eta, \mathbf{k}) - \bar{\rho}_{\mathrm{DR}}(\eta)]/\bar{\rho}_{\mathrm{DR}}(\eta)$.[15] The details of this matching procedure are described in Refs. [16,21,73], giving rise to the initial conditions for the NEDE density contrast $\delta_{\mathrm{NEDE}} \equiv \delta\rho_{\mathrm{NEDE}}/\bar{\rho}_{\mathrm{NEDE}}$ and velocity divergence θ_{NEDE} valid in synchronous gauge (following the definitions in Ma and Bertschinger [74]),

$$\delta_{\mathrm{NEDE}}^{(+)} = -3(1 + w^{(+)})\mathcal{H}_* \frac{\delta q_*}{\bar{q}'_*}$$
$$= \frac{3}{4}(1 + w^{(+)})\delta_{\mathrm{DR}}^*, \qquad (34\mathrm{a})$$

$$\theta_{\mathrm{NEDE}}^{(+)} = k^2 \frac{\delta q_*}{\bar{q}'_*} = -\frac{k^2}{4\mathcal{H}_*}\delta_{\mathrm{DR}}^*, \qquad (34\mathrm{b})$$

where $\mathcal{H} = aH$, primes denote derivatives with respect to conformal time η, and $(+)$ indicates evaluation right *after* the phase transition. The variable $q(\eta, \mathbf{x}) \equiv \bar{q}(\eta) + \delta q(\eta, \mathbf{x})$ defines a general transition surface leading to

spatial trigger time variations $\delta\eta(\mathbf{x}) = -\delta q_*/\bar{q}'_*$. In accordance with the discussion in the previous sections, in the case of hot NEDE, a surface of constant temperature corresponds to a surface of constant tunneling probability. We thus identify $q_*(\mathbf{x})$ with the dark sector temperature $T_d(\eta_*, \mathbf{x})$. This allows us to relate

$$\frac{\delta q_*}{\bar{q}'_*} = -\frac{1}{\mathcal{H}_*}\frac{\delta T_d^*}{T_d^*} = -\frac{1}{4\mathcal{H}_*}\delta_{\mathrm{DR}}^*, \qquad (35)$$

which was used in (34). In a scenario like ours where all the latent heat is converted to radiation, we have $w(a \geq a_*) \simeq 1/3$. As a result, $\delta_{\mathrm{NEDE}}^{(+)} \simeq \delta_{\mathrm{DR}}^*$ and $\theta_{\mathrm{NEDE}}^{(+)} \simeq -k^2\delta_{\mathrm{DR}}^*/(4\mathcal{H}_*)$. It is the latter condition that leads to the matching's distinct imprint on subhorizon scales. We stress that this makes the hot NEDE phenomenology differ from the SIDR case for modes that have entered the horizon before the phase transition. In particular, as discussed in a related context for the acoustic dark energy model [70] but also for cold NEDE [21], the pressure perturbations associated with these dark sector acoustic oscillations will lead to an excess decay of the gravitational potential, which in turn affects structure formation and hence the matter power spectrum at a later stage.

For their subsequent time evolution, we use the continuity and Euler equation in synchronous gauge [74–76],

$$\delta'_{\mathrm{NEDE}} = -(1 + w)\left(\theta_{\mathrm{NEDE}} + \frac{h'}{2}\right)$$
$$- 3\mathcal{H}(c_s^2 - w)\delta_{\mathrm{NEDE}}, \qquad (36\mathrm{a})$$

$$\theta'_{\mathrm{NEDE}} = \frac{k^2 c_s^2}{1 + w^2}\delta_{\mathrm{NEDE}} - \mathcal{H}(1 - 3c_s^2)\theta_{\mathrm{NEDE}}, \qquad (36\mathrm{b})$$

where h is the spatial trace of the metric perturbation, and the sound speed $c_s(a)$ is defined in (B15). The self-interaction required to suppress higher moments and ensure fluidlike behavior is naturally realized within the dark sector model by the residual gauge interactions of the $SU(N - 1)$ group after the phase transition as well as the $\psi \leftrightarrow AA$ process discussed above.

IV. COSMOLOGICAL PARAMETER EXTRACTION

A. Implementation and datasets

We implemented the phenomenological model described in the previous sections into TRIGGERCLASS,[16] which builds on the Cosmic Linear Anisotropy Solving System (CLASS) [76]. The background radiation fluid that triggers the NEDE phase transitions is initialized with a fiducial dark sector temperature $\xi = 0.1$ to ensure the suppression of ΔN_{BBN}. As previously mentioned, this initial dark sector is very

---

[14]For concreteness, a sufficient condition for the absence of any direct bubble signature in CMB data is [21] $H_*/\beta \ll 0.01(z_*/5000)$ (see also Ref. [71] for a recent discussion). According to (20), this condition only requires $g \lesssim \mathcal{O}(1)$ even for a z_* as low as 10^4.

[15]This instantaneous matching approach has also been shown to work in an inflationary context where the inflation sets the initial perturbations in the cosmic fluid after reheating [72]. The main conceptual difference here is that we must also track subhorizon modes as our phase transition occurs at a later time when observable scales have already started to enter the horizon.

[16]https://github.com/NEDE-Cosmo/TriggerCLASS.

subdominant, and its temperature has no impact for observations. Nevertheless, its perturbations play an important role for triggering the perturbations of the dark sector fluid after the phase transition. The first step in ΔN_{eff} is characterized by its redshift z_* and latent heat fraction f_{NEDE} [fixing ΔN_{NEDE} via (27)]. Similarly, the second step is determined by its redshift z_t and size r_g [fixing ΔN_{IR} through (29)]. At the level of perturbations, the trigger fluid is initialized as a tightly coupled radiation plasma with adiabatic perturbations δ_{DR} and θ_{DR}, which are evolved using the standard fluid perturbation equations with $w = c_s^2 = 1/3$. The matching across the transition surface uses (34) to initialize the NEDE perturbations δ_{NEDE} and θ_{NEDE}, which are subsequently integrated using the system (36) (with more details provided in Appendix B). In total, this extends ΛCDM by four parameters: f_{NEDE}, z_*, r_g, and z_t. However, for reasons that will become clear later, we fix $r_g = 0$ (which renders z_t unconstrained) and $z_* = 10^6$ in most of our analysis, which leaves us with f_{NEDE} (or ΔN_{NEDE} equivalently) as the only parameter. We will compare our model with the SIDR model, which extends ΛCDM with ΔN_{eff} as one parameter. The strongly coupled nature of the Dark radiation (DR) component is, as usual, implemented by using a fluid description with vanishing shear.

For the Markov chain Monte Carlo analysis, we use the PYTHON code MONTEPYTHON [77,78] interfaced with TRIGGERCLASS and run the Metropolis Hastings algorithm. We vary all six ΛCDM parameters, i.e., the dimensionless dark matter and baryon densities ω_{cdm} and ω_{b}, the dimensionless Hubble parameter h, the reionization depth τ_{reio}, and the spectral tilt and amplitude n_s and A_s with standard prior choices. We further impose the prior $0 < f_{\mathrm{NEDE}} < 0.3$ and if applicable also $2 < \log_{10}(z_*) < 6$, $0 < \log_{10}(z_*/z_t) < 3$, and $-2 < \log 10(r_g) < 3$. We consider chains to be converged when the Gelman-Rubin parameter satisfies $R - 1 < 0.05$. All neutrinos are effectively treated as massless by setting $N_{\mathrm{eff}} = 3.044$. Unless stated otherwise, we have used the CLASS interpolation table, computed with PARTHENOPE V1.0 [79], to infer the primordial helium abundance Y_p as a function of $N_{\mathrm{eff}}^{\mathrm{BBN}} \equiv 3.044 + \Delta N_{\mathrm{BBN}}$ and $\omega_b h^2$.

We use the following datasets for our analysis[17]:

(i) *Planck 2018*. The combined Planck 2018 lensing, high-ℓ TT + TE + EE, and low-ℓ TT + EE CMB anisotropy measurements [80,81].

(ii) *Baryon acoustic oscillations*: We include three baryon acoustic oscillation (BAO) measurements from 6dF Galaxy Survey (6dFGS) at $z = 0.106$ [82], Sloan Digital Sky Survey (SDSS) at $z = 0.15$ [83],

and also SDSS-III DR12 at $z = 0.38$, 0.51, 0.61 [84].

(iii) *Pantheon*: The "Pantheon Sample" luminosity distances of Supernovae (SNe) Ia covering the redshift range $0.01 < z < 2.3$ [85].

(iv) *SH0ES*: To assess the ability of the model to address the H_0 tension, in addition to our main analysis, we also use the SH0ES results from the Cepheid–SN Ia sample at $z < 0.01$ to put priors on the Hubble parameter $h = 0.7304 \pm 0.0104$ [86].

(v) *BBN*: We include the BBN information in the form of a prior on $\Delta N_\nu^{\mathrm{BBN}} = 2.889 \pm 0.229$ obtained from helium and deuterium abundance measurements [32], noticing that this result is CMB independent, i.e., it does not include the CMB measurements of the baryon abundance or use the CMB constraint on ΔN_{eff}.[18]

We refer to Planck 2018, BAO, and Pantheon as our "base" dataset. When quantifying the Hubble tension, we will use the *difference of the maximum a posteriori* measure

$$Q_{\mathrm{DMAP}}(H_0) = \sqrt{\chi^2_{\mathrm{w}\backslash\mathrm{H}_0} - \chi^2_{\mathrm{w}\backslash\mathrm{o}\,\mathrm{H}_0}}. \qquad (37)$$

Following Ref. [87], we compute it as the root square of the difference between the best-fit χ^2 values with and without the SH0ES prior on H_0 included. We further employ the Akaike Information Criterion [88] $\Delta\mathrm{AIC} = \Delta\chi^2 + 2 \times$ (#added parameters) for model comparison.

B. Results

Before presenting results for the hot NEDE model, we first discuss the impact of taking into account BBN constraints on ΔN_{eff} and Y_p within SIDR. The purpose of this exercise is to quantify in how far models that do *not* feature a post-BBN heating mechanism are disfavored when it comes to the H_0 tension.

1. SIDR

Different variants of the stepped and nonstepped SIDR model have been investigated rather extensively in the literature as a possible solution to the Hubble tension [8,9,11,89–92]. Therefore, it is not our ambition here to repeat these analyses or add to the controversy about their effectiveness as solutions to the Hubble tension when BBN constraints are absent (for extensive recent studies, see Refs. [11,91]). Instead, we will focus on a rather basic SIDR model without dark matter interactions and mass threshold and with constant ΔN_{eff} throughout the relevant BBN and recombination epochs. We add a BBN constraint on ΔN_{eff} to the base datasets when analyzing the SIDR model. Our corresponding results are summarized in Fig. 3. We see that including the BBN constraint on ΔN_{eff} (orange

---

[17]Here, we closely follow the datasets considered in Ref. [8], leaving the inclusion of information about the full-shape of the matter power spectrum, redshift space distortions, and additional ground-based CMB data for future work.

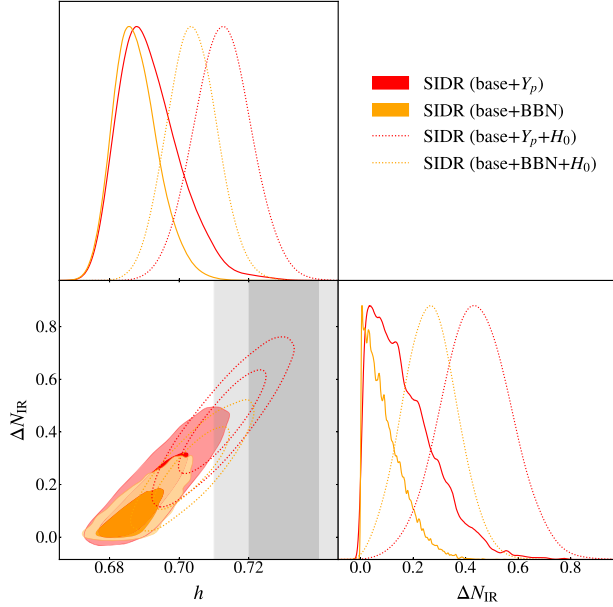[18]We use the relation $\Delta N_{\mathrm{eff}} = (1.0147)\Delta N_\nu^{\mathrm{BBN}}$.

FIG. 3.   Impact of BBN constraint on a simple SIDR model with constant $\Delta N_{\rm eff}$. Orange contours show 68% C.L. and 95% C.L. marginalized posteriors when including the BBN prior on $\Delta N_{\rm eff}$ and using the corresponding helium abundance predicted by BBN. The red contours show for comparison the case when ignoring BBN constraints and setting the helium fraction to the value found for ΛCDM ($Y_p = 0.2454$) by hand, as done in previous analyses. Filled contours correspond to the case without SH0ES, and open dotted contours illustrate the impact of including SH0ES. We observe that BBN disqualifies SIDR models without a post-BBN heating mechanism for addressing the H_0 tension.

contour) makes the SIDR model *incompatible* with the SH0ES value of H_0 (gray vertical band). This corresponds to a residual difference of the maximum a posteriori (DMAP) tension of 3.9σ (only slightly improving on the ΛCDM tension of 4.3σ). Correspondingly, the fit improvement over ΛCDM remains relatively small with $\Delta\chi^2 = -4$ when the analysis includes the (incompatible) H_0 prior. These findings clearly remove the simple SIDR model from the space of interesting proposals to resolve the Hubble tension. Let us stress that similar conclusions were reached for the stepped SIDR model when BBN constraints were included [9]. Nevertheless, most of the previous studies on the (stepped) SIDR solutions find smaller values for the residual tension as they neither infer Y_p from BBN nor impose constraints on $\Delta N_{\rm eff}$. However, we take the point of view that a viable model should be able to describe both the BBN and CMB epochs, since they interfere in multiple ways. This motivates models featuring a post-BBN heating mechanism such as the hot NEDE scenario investigated in this work, to which we turn next.

2. Hot NEDE

In the hot NEDE model, $N_{\rm BBN} \simeq 3.044$ during BBN and thus including the BBN constraint does not lead to any
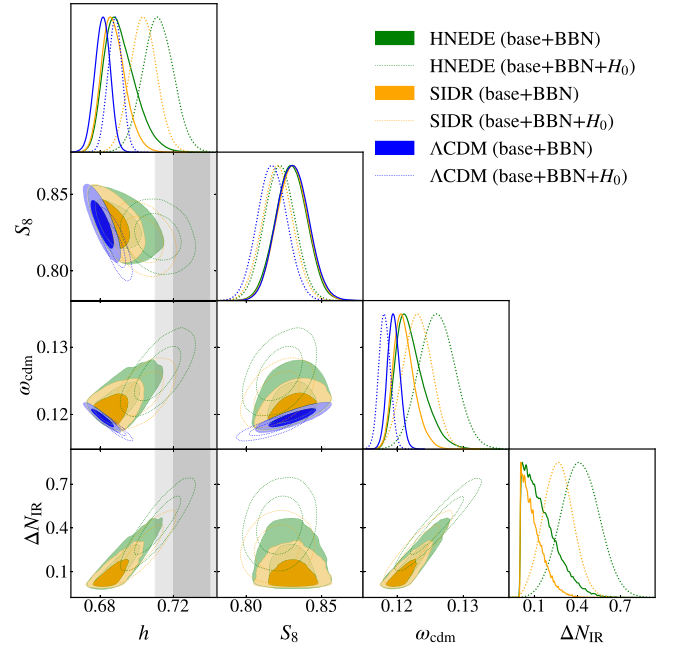

FIG. 4.   Comparison between the ΛCDM (blue), SIDR (orange), and HNEDE (green) 68% C.L. and 95% C.L. marginalized posteriors, with BBN information included in all cases and without (filled) and with (open dotted) including SH0ES. Only HNEDE is marginally compatible with the SH0ES value of h (gray vertical band).

penalty. Thus, while both the hot NEDE setup studied in this work as well as SIDR lead to a similar $\Delta N_{\rm eff}$ around recombination, the BBN constraint hardly affects the posteriors within hot NEDE, and (as expected) merely creates a small, data-insensitive offset $\Delta\chi^2_{\rm BBN} = 0.23$.

We provide a comparison between the ΛCDM, hot NEDE, and SIDR posteriors in Fig. 4, with the dashed contours representing the addition of the H_0 prior. We find that hot NEDE provides the larger values of H_0, *when including BBN information*. As the main result, described in Tables III and IV, we find that the DMAP tension is reduced to 2.8σ (which should be compared to 3.9σ for the SIDR model). In the absence of the SH0ES prior on H_0, we obtain $H_0 = 69.13^{+0.62}_{-1.0}$ km sec^{-1} Mpc^{-1} (68% C.L.), which translates into a Gaussian tension of 3.2σ. This is slightly higher than the DMAP tension of 2.8σ, which we attribute to the non-Gaussian shape of the posterior. On the other hand, if we include the SH0ES prior, we find $\Delta N_{\rm IR} = 0.42 \pm 0.13$ (68% C.L.), which corresponds to a larger than 3σ preference for hot NEDE over ΛCDM. While the model in this simple form is arguably not a full resolution of the Hubble tension, our point here is that the model remains in the space of *possible* solutions, whereas DR models susceptible to the BBN constraint are not. Here, we consider a simple and minimal model, and we leave for future work investigating extended versions that, for example, feature interactions between the dark radiation and dark matter components.

TABLE III. Summary of results for our combined analyses (with and without a SH0ES prior on H_0). We compare ΛCDM, SIDR, and HNEDE (with negligible second step, i.e., $r_g = 0$). If applicable, we present the mean values with $\pm 1\sigma$ error. As a result of including the BBN constraints, the SIDR model is hardly an improvement over ΛCDM.

| | Base + BBN | | | | | $+H_0$ | | | | | |
	H_0	ΔN_{IR}	χ^2	$\Delta\chi^2$	ΔAIC	H_0	ΔN_{IR}	χ^2	$\Delta\chi^2$	ΔAIC	$\sqrt{Q_{DMAP}^{H_0}}$
ΛCDM	68.13 ± 0.42	$\cdots$	3810.5	$\cdots$	$\cdots$	68.81 ± 0.39	$\cdots$	3829.7	$\cdots$	$\cdots$	4.3σ
SIDR	$68.77^{+0.52}_{-0.73}$	$0.094^{+0.024}_{-0.093}$	3810.5[a]	0.0	2.0	70.37 ± 0.72	0.27 ± 0.10	3825.7	-4.0	-2.0	3.9σ
Hot NEDE	$69.13^{+0.62}_{-1.0}$	$0.151^{+0.041}_{-0.15}$	3810.4	-0.1	1.9	71.17 ± 0.83	0.42 ± 0.13	3818.3	-11.4	-9.4	2.8σ

[a]Here we take the ΛCDM value as bestfit, since we were not able to find the bestfit for SIDR with the base datasets.

TABLE IV. Detailed comparison of the bestfit χ^2 for different datasets and models, including BBN information in all cases. For hot NEDE, we also include the case when allowing for the second step in the last column, which performs similarly to our fiducial analysis with $r_g = 0$. Note that we do not include the case with free z_*, since it is very similar to the fiducial scenario with $z_* = 10^6$. The SIDR model without H_0 prior is also not shown; see Table III.

| | ΛCDM | | SIDR | Hot NEDE | | |
	Base + BBN	$+H_0$	Base + BBN + H_0	Base + BBN	$+H_0$	$+H_0, r_g, z_t$
Planck High-ℓ TT-TE-EE	2350.4	2350.6	2354.6	2351.7	2355.1	2353.0
Planck Low-ℓ EE	396.0	398.5	398.1	395.7	395.8	398.3
Planck Low-ℓ TT	23.7	23.0	22.3	22.7	22.2	21.5
Planck lensing	8.8	8.6	8.9	8.9	9.2	9.4
BAO	5.2	6.1	6.0	5.2	6.2	7.2
SH0ES	$\cdots$	15.6	7.2	$\cdots$	3.7	1.5
Pantheon	1025.9	1026.6	1025.77	1025.7	1025.6	1026.1
BBN	0.2	0.2	2.5	0.2	0.2	0.2
Total	3810.5	3829.7	3825.7	3810.4	3818.3	3817.5

A further interesting feature that can be observed in Fig. 4 is that for the hot NEDE model and the base + BBN dataset S_8 slightly decreases when increasing h. We checked that this can be attributed to a decrease in the matter density parameter $\Omega_m = (\omega_{cdm} + \omega_b)/h^2$ entering $S_8 = \sigma_8\sqrt{\Omega_m/0.3}$, while the clustering amplitude on scales of $8 \, h/$Mpc, σ_8, stays approximately constant or even slightly increases with h. The decrease of Ω_m is a consequence of an overcompensation of the increase of ω_{cdm} due to the factor $1/h^2$. We note that these features could be interesting to investigate further in view of the S_8 tension reported by weak lensing shear measurements; see, e.g., Ref. [93] for a recent analysis.

We note that, when choosing the redshift of the phase transition $z_* \gtrsim 10^5$ such that modes affecting the CMB were still outside the horizon at z_*, we expect that the hot NEDE model yields results that are comparable to previous analyses of SIDR models that had ignored BBN constraints. We find that this is indeed true for our fiducial choice $z_* = 10^6$. Comparing the green contours in Fig. 4

with the red ones in Fig. 3, we see that there is almost no discernible difference between both models *when the BBN constraint on SIDR is removed*.[19]

Similarly, data are also not able to meaningfully constrain the second step (green contour in Fig. 8). This is broadly in agreement with the findings in Ref. [11], although it is possible that in a slightly more sophisticated scenario with dark matter interactions the step feature can be more clearly constrained. Moreover, in Ref. [11], it was found that the Q_{DMAP} tension measure hints at a more favorable effect the step has on the Hubble tension, in line with Ref. [8]. As this is not the focus of the current analysis, we leave this question for future explorations and, for simplicity, set $r_g = 0$ (which also renders z_t unconstrained). For a broader discussion on the second step, see Appendix A.

Moreover, as we demonstrate in Fig. 5, data provide us with a lower bound $\log_{10}(z_*) > 4.64$ (95% C.L.) (orange

---

[19]This also serves as a nontrivial cross-check of how we initialize perturbations in the NEDE fluid on superhorizon scales.
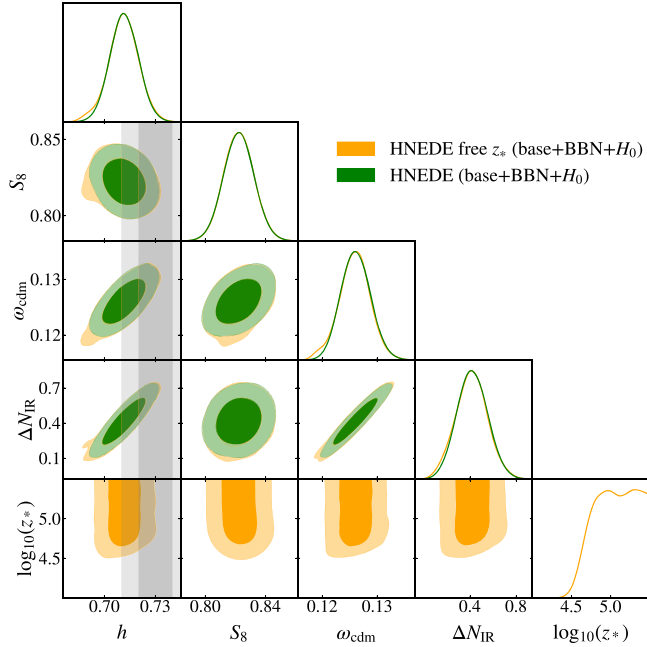
FIG. 5. Posteriors when including the redshift of the dark sector phase transition z_* as a free parameter, compared to the fiducial case with fixed $z_* = 10^6$. Including z_* does not affect the posteriors of the other model parameters and provides us with a lower bound $z_* > 4.4 \times 10^4$ (95% C.L.).

contour). This is an important result, as it yields a wide window (roughly five orders of magnitude in redshift) between BBN and $z = 4.4 \times 10^4$ during which the phase transition can have occurred. We note that this result also highlights the relevance of the trigger physics. For comparison, in the case of cold NEDE, adiabatic perturbations in a slowly rolling scalar field trigger the phase transition; instead, here, this role is played by perturbations in the dark radiation fluid. While this difference in microphysics would not matter on superhorizon scales, it does make a difference on subhorizon scales. Although we do not provide a quantitative exploration, the qualitative explanation is as follows: The thermal trigger enhances the initial conditions for δ_{NEDE} and θ_{NEDE} on scales $k > \mathcal{H}_*$ via (34) [together with (35)]. As a result, these modes will carry rather strong dark acoustic oscillations, which would be incompatible with the CMB if the phase transition would occur at $z_* \lesssim 10^5$. This is illustrated in Fig. 7, where we compare the CMB temperature power spectrum for hot NEDE cosmologies for different values of z_*. However, this conclusion is avoided if the phase transition occurs early enough such that the CMB modes are still frozen on superhorizon scales at z_*. This is different for cold NEDE. Here, the dark acoustic oscillations are moderated by the amount of slow-rolling of the trigger field at the time of the phase transition [21]. In Sec. V B, we argue that the enhanced dark acoustic oscillations imprinted on somewhat smaller

scales than those probed by the CMB are actually an interesting signature of hot NEDE that can be searched for in LSS data, and that further sets it apart from SIDR models.

As a result, we are left with a one-parameter extension of ΛCDM that performs similarly as analyses of the SIDR model when disregarding BBN. When including BBN constraints, hot NEDE remains largely unaffected, while SIDR is disfavored. Thus, the heating by the first-order phase transition provides an efficient mechanism to make models addressing the Hubble tension within an SIDR-like setup consistent with BBN.

V. PHENOMENOLOGY

A vacuum phase transition between BBN and recombination leads to unique signatures. If the phase transition happens early enough with $z_* > 10^6$, there is the prospect of detecting a stochastic background of low-frequency gravitational waves. On the other hand, if it does occur sufficiently late with $z_* < 10^6$, it will imprint itself in the CMB and in the matter power spectrum on small scales. We will discuss these somewhat complementary possibilities in turn.

A. Gravitational waves

A stochastic gravitational wave background is a typical prediction of a cosmological first-order phase transition. In general, there are different production mechanisms, related either to plasma effects such as sound waves and turbulence or the bubble walls. To keep the discussion simple, we will focus here on bubble collisions as the source of gravitational waves (additional sources might lead to a stronger signal [55–61]). In that case, the spectrum produced has a characteristic peak determined by the typical size of the nucleated bubbles relative to the Hubble scale at the time when they collide (we follow Refs. [65,21]),

$$h^2 \Omega_{\text{GW}} = 6 \times 10^{-8} (H_* \beta^{-1})^2$$
$$\times \left(\frac{f_{\text{NEDE}}}{0.1} \right)^2 (g^*_{\text{rel,vis}})^{-1/3} S_{\text{GW}}(f), \quad (38)$$

where β^{-1} sets the timescale for the duration of the transition [see (20)] and the strength of the transition is commonly characterized by $\alpha = \Delta V_* / (\rho^*_{\text{rad,d}} + \rho^*_{\text{rad,vis}})$, which implies $\alpha = f_{\text{NEDE}} / (1 - f_{\text{NEDE}})$ [see (17)]. Further,

$$S_{\text{GW}}(f) \simeq \frac{3.8 (f/f_*)^{2.8}}{1 + 2.8 (f/f_*)^{3.8}} \quad (39)$$

is the spectral shape obtained in the envelope approximation [94] (see also Refs. [94–100]), and
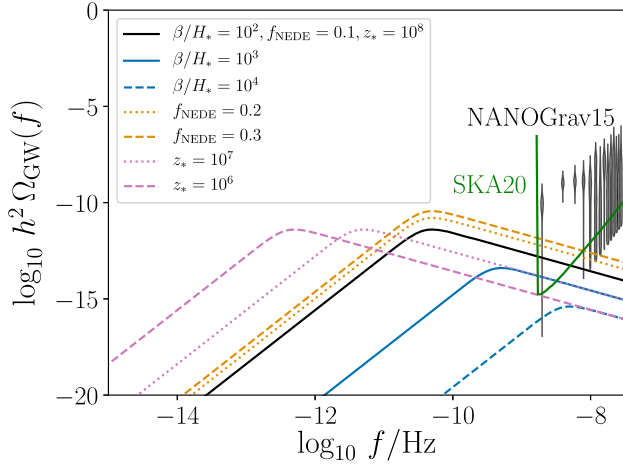
FIG. 6. Gravitational wave spectrum generated in the first-order phase transition using the envelope approximation. We show an estimated prediction for a benchmark scenario (black) and the impact when varying one of the parameters (other lines; see legend). We also include NANOGrav 15-year results from Ref. [105] and the expected sensitivity of SKA after 20 years of data.

$$f_* \simeq 4.1 \times 10^{-6} \text{ nHz} \frac{1}{(H_*\beta^{-1})}\left(\frac{1+z_*}{10^6}\right)(g^*_{\text{rel,vis}})^{1/6} \qquad (40)$$

is the peak frequency as measured today. Before the peak, the spectrum grows as f^3 for $f \ll f_*$ and falls off after the peak as f^{-1} for $f \gg f_*$. Even in the extreme case where the phase transition happens just after BBN, with $z_* \lesssim z_{\text{BBN}} \sim 10^9$, the peak frequency is smaller than nanohertz. Therefore, only in the regime $f \gg f_*$, we can have hope of detecting a signal with pulsar timing arrays probing $f \sim$ nHz [101]. To find the amplitude of the signal in the nanohertz regime, one can substitute (40) into (38),

$$\Omega_{\text{GW}}h^2 \simeq 3.4 \times 10^{-13}\left(\frac{H_*\beta^{-1}}{0.01}\right)\left(\frac{\text{nHz}}{f}\right)$$
$$\times \left(\frac{f_{\text{NEDE}}}{0.1}\right)^2 (g^*_{\text{rel,vis}})^{-1/6}\left(\frac{1+z_*}{10^8}\right), \qquad (41)$$

where the ratio H_*/β, due to (20), is bounded from above by 10^{-2} (corresponding to an order unity gauge coupling). For example, given the peak frequency of the *Square Kilometer Array* (SKA) of [102–104] $\Omega_{\text{GW}}h^2 \sim 10^{-15}$, we could expect a signal for a phase transition that occurs in the range $z_{\text{BBN}} > z \gtrsim 10^6$. We display in Fig. 6 some scenarios for the gravitational wave prediction from the envelope approximation, together with results from 15 years of pulsar observations by the NANOGrav Collaboration [105] as well as the expected sensitivity of SKA after 20 years of observation.[20]

---

[20]For a detailed analysis of a pre-BBN phase transition in a dark sector including BBN constraints on N_{eff}, see Ref. [106] (see also Ref. [25] for a discussion of how these constraints can be avoided).

We stress that the falloff in (39) is obtained by using the envelope approximation, which is subject to rather large theoretical uncertainties. In particular, recent lattice calculations indicate that the falloff lies between [107,108] $f^{-1.4}$ and $f^{-2.2}$, which for a post-BBN phase transition with $z_* \lesssim 10^9$ would move a signal below the sensitivity threshold. However, the same studies also find the presence of a "bump" in the high-frequency tail. It is caused by oscillations of the scalar field around the true vacuum and can raise the power even above the envelope estimate. Moreover, it is not clear if these studies account for the phenomenology of a supercooled phase transition. We therefore leave a more detailed discussion of these issues for future work and maintain that Fig. 6 can still provide us with an indication of where to look for a signal.

B. Small scales

The first-order phase transition imprints characteristic features on the small-scale matter power spectrum, affecting modes that have already entered the horizon at the transition z_*, i.e., on scales

$$k \gtrsim \frac{0.3h}{\text{Mpc}}\frac{1+z_*}{10^5}. \qquad (42)$$

As discussed in Secs. IV B and III E, the adiabatic perturbations present in the dark radiation trigger the phase transition at slightly different times in different locations and kick off fluctuations on the dark plasma after the transition on subhorizon scales whose propagation leads to dark acoustic oscillations. Since the dark radiation constitutes a non-negligible fraction of the energy density *after* the transition, $\rho_{\text{NEDE}}/\rho_{\text{vis}} \simeq 8\% \times (\Delta N_{\text{eff}}/0.6)$, they impact the gravitational potential and consequently imprint oscillatory features on the CMB as well as on the matter power spectrum;; see Fig. 7. For $z_* = 10^4$, these features overlap with the scales probed by the CMB, excluding these low redshifts, requiring $z_* \gtrsim 4 \times 10^4$ as discussed in Sec. IV B. However, for $z_* \sim 10^5$–10^6, the dark acoustic oscillations show up on smaller scales $k \gtrsim 0.3 \, h/\text{Mpc}$ where they can potentially be probed by large-scale structure observations. We indicate the scales probed by one-dimensional Lyman-α forest measurements by the gray band in Fig. 7, for which the ongoing Dark Energy Spectroscopic Instrument (DESI) survey [109] is expected to achieve percent-level sensitivity [110,111]; see [112] for first results from the early data release. We also show the power spectrum for the case with the same amount of DR but without phase transition (SIDR) in Fig. 7 for comparison, that is likely indistinguishable from ΛCDM. Thus, small-scale probes of the power spectrum may discriminate SIDR from the hot NEDE scenario if the phase transition occurs for $10^6 \gtrsim z_* \gtrsim 10^5$.
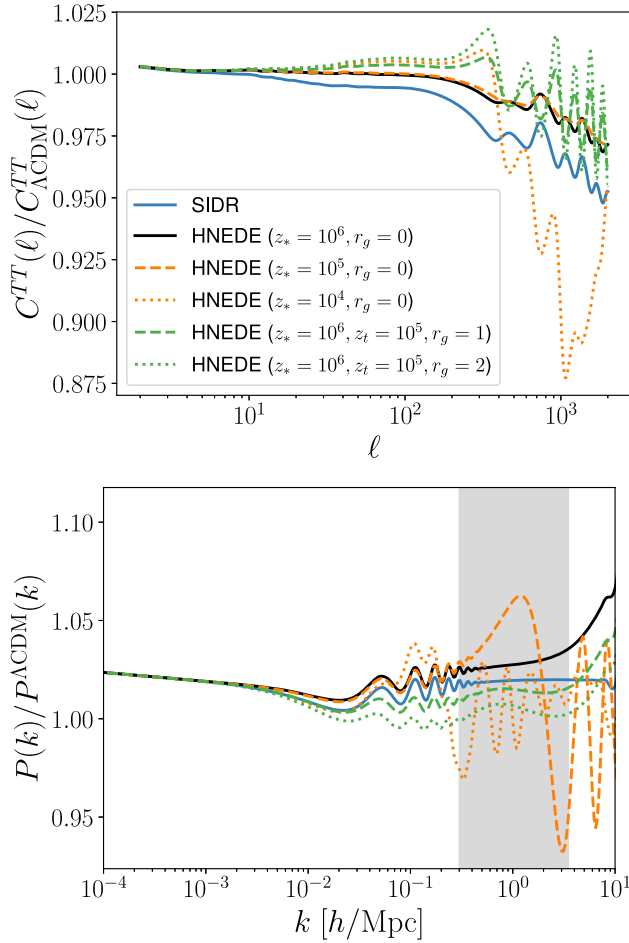
FIG. 7. CMB C_ℓ^{TT} (upper panel) and matter power spectra $P(k)$ (lower panel) for HNEDE models with various z_* and r_g, normalized to ΛCDM. In all cases, we use the best-fit (base + BBN + H_0) parameters obtained for HNEDE with $z_* = 10^6$, $r_g = 0$ and match $\Delta N_{\rm IR} = 0.40$ for SIDR. Compatibility with Planck requires $z_* \gtrsim 10^5$, while for $z_* \lesssim 10^6$, Lyman-α scales overlap with the onset (yellow dashed) or even the first peaks (yellow dotted) of the dark sector acoustic oscillations. The gray area represents the region probed by Lyman-α forest data.

VI. CONCLUSION

In this work, we point out a conceptually simple model that can address the Hubble tension by adding extra dark radiation around recombination, while retaining the success of BBN. Its central feature is a supercooled first-order phase transition that occurs in a dark sector between the BBN and recombination epochs. The latent heat released in the phase transition heats up the dark sector, such that the amount of extra radiation can be sizeable during recombination while it is negligibly small during BBN.

We find that all properties of such a dark sector that are favorable from the point of view of cosmology can be realized within a straightforward microscopic model. It features a (dark) gauge symmetry that is spontaneously broken as $SU(N) \to SU(N-1)$ by a scalar field. The

associated phase transition is of first order and features strong supercooling if the scalar is described by a classically (nearly) scale-invariant Lagrangian, leading to radiative symmetry breaking *à la* Coleman-Weinberg in the limit of vanishing effective mass of the scalar field. A soft mass term breaking scale-invariance provides a natural graceful exit mechanism to terminate the supercooling phase and alongside a well-tempered amount of latent heat.

Moreover, the dark radiation after the transition is composed of the massless gauge bosons belonging to the remaining $SU(N-1)$ symmetry as well as the light dark Higgs boson also characteristic of the Coleman-Weinberg mechanism. The $SU(N-1)$ gauge interactions naturally make the dark radiation strongly interacting, thus realizing SIDR. Moreover, once the light Higgs becomes nonrelativistic somewhat after the phase transition, another slight increase of the amount of extra radiation occurs, as considered in the stepped SIDR scenario. This model thus naturally connects the previously discussed frameworks with hot NEDE, thereby UV completing (stepped) SIDR to achieve a consistent cosmological model for addressing the Hubble tension while allowing us to also embrace BBN.

To demonstrate the effectiveness of this setup, we implemented the model in a Boltzmann solver and performed an analysis of Planck CMB, as well as BAO and SNe Ia data, considering in addition a prior on the amount of radiation during BBN. This also allows us to consistently use the prediction of the helium fraction from BBN for the subsequent recombination dynamics. We find that for the model considered in this work the Hubble tension can be reduced to the level of 2.8σ, while for SIDR, we find 3.9σ due to the penalty from spoiling BBN (for comparison, our analysis yields 4.3σ for ΛCDM). We note that, when ignoring BBN, SIDR performs similarly to the model considered here.

The supercooled phase transition between BBN and recombination leads to various signatures. If it occurs shortly after BBN, say for $z_* \sim 10^8$, the stochastic gravitational wave background generated by the transition can potentially be seen in pulsar timing arrays, even though a robust prediction would require further work. If the phase transition occurs in the range $10^6 \gtrsim z_* \gtrsim 10^5$, the impact of dark acoustic oscillations triggered by the transition can be probed with future DESI Lyman-α forest data. We also find a lower bound $z_* \gtrsim 4 \times 10^4$ from Planck CMB data, since otherwise the dark oscillations would affect the high-ℓ modes. We find the hot NEDE perturbations triggered by the dark plasma to be stronger compared to the case of a scalar-field induced (cold NEDE) transition for modes that are already subhorizon at z_*.

Our work motivates further exploration, including technical improvements, for example, related to the thermalization dynamics immediately after the transition and the gravitational wave production and spectrum (including sound waves), as well as phenomenological aspects. To be concrete, it would be interesting to investigate connections with dark matter, e.g., dark matter production in the phase transition [44] or the possibility that dark matter is charged under the dark $SU(N)$, which may also address the

S_8 tension seen in various weak lensing datasets via scattering of dark matter with dark radiation [6,16], which may lead to further signatures in galaxy clustering [90,113] or cluster counts [114]. Another direction could be the dynamics in the early Universe that is responsible for creating the small initial dark sector temperature prior to the phase transition. We note that even the purely gravitational interactions with the visible sector could be sufficiently strong to provide this initial population [115], with the $SU(N)$ gauge interactions leading to efficient thermalization within the dark sector [67].

APPENDIX A: RESULTS INCLUDING THE SECOND STEP

In this Appendix, we provide further results when explicitly including the second (small) step in $\Delta N_{\rm eff}$ due to the dark Higgs becoming nonrelativistic at some redshift $z_t < z_*$. Such a step was first considered in Ref. [8] as a solution to the Hubble tension (without considering a phase transition at z_*), and we review its dynamics in Appendix B.

We display in Fig. 8 the posteriors when including SH0ES data and considering the second step with size r_g [see (B9)] at redshift z_t, sampled as $\log_{10} r_g$ and $\log_{10} z_*/z_t$, respectively (keeping $z_* = 10^6$ fixed). We find $\log_{10}(r_g) < 1.03$ (95% C.L.) and also a relatively unconstrained redshift z_t for the second step. That is consistent with the findings in Fig. 7, in which we notice that the effect of r_g in the angular power spectrum C^{TT} and in the matter power spectrum $P(k)$ is relatively small. Notice that the second step within the $SU(N)$ model is indeed expected to be small with $r_g \leq 1/6$ in agreement with the phenomenological bound. This can be compared with the Wess Zumino Dark Radiation (WZDR) model in Ref. [8], which predicts $r_g^{\rm WZDR} = 8/7$. However, this model suffers from BBN constraints similarly to the simplest SIDR model discussed in the main text.

Note that within the $SU(N)$ model the redshift of the second step, as derived in (31), is theoretically constrained to occur within a few e-folds after the phase transition, depending on the gauge coupling g. In contrast, the step size r_g depends only on the size N of the gauge group. More precise high-ℓ CMB data may be able to discriminate scenarios with different step size and redshift, which would therefore allow to specifically constrain N and g, respectively.
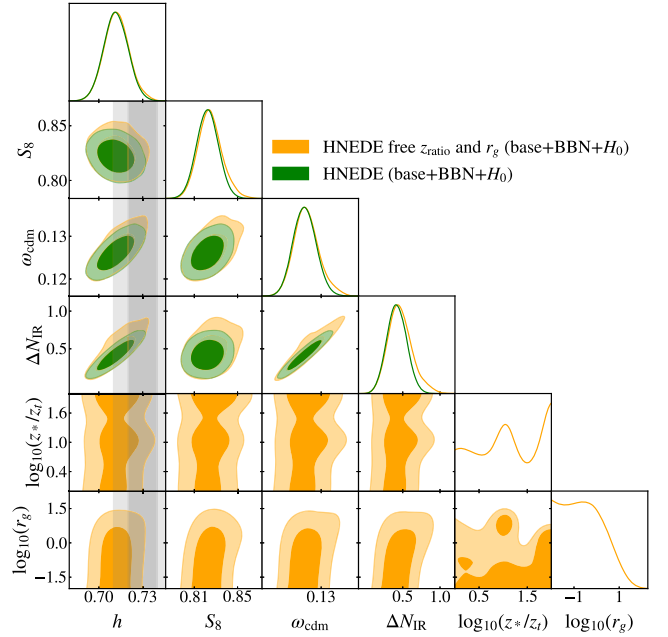

FIG. 8. Posteriors exploring the second step at redshift z_t for which the dark Higgs becomes nonrelativistic after the phase transition at z_* in the HNEDE model. We compare the model considered in the main text with step size $r_g = 0$ (green contours) and another one where r_g and z_t are sampled (orange contours). While r_g is bounded from above, z_t is hardly constrained at all, in agreement with findings in the literature for stepped SIDR models [11].

APPENDIX B: REVIEW OF FORMALISM FOR THE SECOND STEP

In this Appendix, we review the dynamics of the second step, following Ref. [8]. The expressions are used for our CLASS implementation of the dynamics around z_t within hot NEDE. We consider a dark sector Higgs field with g_h degrees of freedom ($g_h = 1$ in our model), mass m, temperature T_d, and vanishing chemical potential[21] and use the dimensionless variable

$$x(a(t)) = m/T_d(a(t)). \tag{B1}$$

We first recall the expressions for the Maxwell-Boltzmann and Bose-Einstein distributions with vanishing chemical potential for a single degree of freedom,

$$\rho_{\rm MB}(T_d) = \int_{\boldsymbol{q}} \sqrt{q^2 + m^2} e^{-\sqrt{q^2 + m^2}/T_d}$$
$$= \frac{3T_d^4}{\pi^2}\left(\frac{K_1(x)}{6}x^3 + \frac{K_2(x)}{2}x^2\right),$$
$$\rho_{\rm BE}(T_d) = \int_{\boldsymbol{q}} \sqrt{q^2 + m^2}[e^{\sqrt{q^2 + m^2}/T_d} - 1]^{-1}, \tag{B2}$$

---

[21]The gauge bosons interactions fix $\mu_{\rm gauge} = 0$, and the Higgs gauge boson interactions set $\mu_h = 2\mu_{\rm gauge}$.

where $\int_q \equiv \int \frac{d^3q}{(2\pi)^3}$, and K_i are the modified Bessel functions of the second kind. Similar expressions can be obtained for the pressure. In the high-temperature limit $T_d \gg m$,

$$\rho_{\mathrm{MB}}^{\mathrm{highT}}(T_d) = \frac{3}{\pi^2} T_d^4,$$

$$\rho_{\mathrm{BE}}^{\mathrm{highT}}(T_d) = \frac{\pi^2}{30} T_d^4, \qquad (\mathrm{B3})$$

with $\rho^{\mathrm{highT}}(T_d) = 3p^{\mathrm{highT}}(T_d)$ for both statistics. We define the (dimensionless) normalized density and pressure for the Maxwell-Boltzmann statistics as

$$\hat{\rho}(T) \equiv \rho_{\mathrm{MB}}(T)/\rho_{\mathrm{MB}}^{\mathrm{highT}}(T) = \frac{K_1(x)}{6} x^3 + \frac{K_2(x)}{2} x^2,$$

$$\hat{p}(T) \equiv p_{\mathrm{MB}}(T)/p_{\mathrm{MB}}^{\mathrm{highT}}(T) = \frac{K_2(x)}{2} x^2. \qquad (\mathrm{B4})$$

Following Ref. [8], we approximate the dark Higgs density and pressure as

$$\rho_h(T_d) \equiv g_h \rho_{\mathrm{BE}}^{\mathrm{highT}} \hat{\rho}_{\mathrm{MB}}(T_d), \qquad (\mathrm{B5})$$

$$p_h(T_d) \equiv g_h p_{\mathrm{BE}}^{\mathrm{highT}} \hat{p}_{\mathrm{MB}}(T_d). \qquad (\mathrm{B6})$$

Notice that, in the limit $T_d \gg m$, one has $\hat{\rho}(T) \to 1$ and $\rho_h(T) \to g_h \rho_{\mathrm{BE}}^{\mathrm{highT}}$. In other words, the approximation is normalized such that it reproduced the correct quantum statistical result in the high-T limit. It slightly deviates from quantum statistics in the low-T regime [8], where the distribution is already Boltzmann suppressed.

The total dark sector density and pressure at $z < z_*$, including also the massless $SU(N-1)$ gauge bosons after the phase transition, can be written as

$$\rho_d(T_d) = \rho_h(T_d) + \frac{\pi^2 g_{\mathrm{gauge}} T_d^4}{30}$$

$$= \frac{\pi^2 g_{\mathrm{gauge}} T_d^4}{30}(1 + r_g \hat{\rho}(x)), \qquad (\mathrm{B7})$$

$$p_d(T_d) = p_h(T_d) + \frac{\pi^2 g_{\mathrm{gauge}} T_d^4}{90}$$

$$= \frac{\pi^2 g_{\mathrm{gauge}} T_d^4}{90}(1 + r_g \hat{p}(x)), \qquad (\mathrm{B8})$$

where g_{gauge} is the number of relativistic degrees of freedom in the gauge sector, with the same dark temperature T_d, and

$$r_g \equiv \frac{g_h}{g_{\mathrm{gauge}}}, \qquad (\mathrm{B9})$$

following the notation used in Ref. [8] for the corresponding quantity. For the dark sector with $SU(N) \to SU(N-1)$ symmetry breaking, we have $g_h = 1$ and $g_{\mathrm{gauge}} = 2N(N-2)$, i.e. $1/6 \geq r_g \geq 0$ for $3 \leq N < \infty$. That leads to a substantially smaller step if compared to the WZDR model of Ref. [8], in which $r_g^{\mathrm{WZDR}} = 8/7$.

Parametrizing the energy density in units of the neutrino energy density $\rho_{1\nu} = \frac{7}{4} \frac{\pi^2}{30} (\frac{T_{\nu0}}{a})^4$ via

$$\rho_d(x) \equiv \Delta N_{\mathrm{eff}}(x) \rho_{1\nu}, \qquad (\mathrm{B10})$$

we find after matching with (B7)

$$\Delta N_{\mathrm{eff}}(x) = \Delta N_{\mathrm{IR}} \frac{1 + r_g \hat{\rho}(x)}{[1 + r_g(\frac{3}{4}\hat{\rho}(x) + \frac{1}{4}\hat{p}(x))]^{4/3}}. \qquad (\mathrm{B11})$$

This allows us to identify the effective number of relativistic degrees of freedom before (NEDE) and after (IR) the step as

$$\Delta N_{\mathrm{NEDE}} = \frac{\Delta N_{\mathrm{IR}}}{(1 + r_g)^{1/3}}, \qquad (\mathrm{B12})$$

$$\Delta N_{\mathrm{IR}} = \frac{g_{\mathrm{gauge}}}{7/4} \left(\frac{T_{d0}}{T_{\nu0}}\right)^4. \qquad (\mathrm{B13})$$

Using (B7) and (B8), we obtain for the equation of state and the speed of sound

$$w(x) = \frac{1}{3} - \frac{r_g}{3} \frac{\hat{\rho}(x) - \hat{p}(x)}{1 + r_g \hat{\rho}(x)}, \qquad (\mathrm{B14})$$

$$c_s^2(x) = \frac{1}{3} - \frac{r_g}{3} \frac{\hat{\rho} - \hat{p} - \frac{x}{4}(\hat{\rho}' - \hat{p}')}{1 + r_g \hat{\rho} - \frac{x}{4} r_g \hat{\rho}'}. \qquad (\mathrm{B15})$$

In order to derive $x(a)$, needed for the Boltzmann implementation, we use entropy conservation within the dark sector for $z > z_*$, implying $x \times (\rho + p) \propto 1/a^3$. This can be written as

$$\left(\frac{xa_t}{a}\right)^3 = 1 + \frac{r_g}{4}(3\hat{\rho}(x) + \hat{p}(x)) \qquad (\mathrm{B16})$$

and solved for a

$$a = a_t x \left(\frac{1}{1 + \frac{r_g}{4}[3\hat{\rho}(x) + \hat{p}(x)]}\right)^{1/3}, \qquad (\mathrm{B17})$$

where $a_t \equiv 1/(1 + z_t)$ is the scale at which the Higgs field becomes nonrelativistic as defined in Ref. [8] and used as an input parameter for the Boltzmann solver in the form of $z_{\mathrm{ratio}} = z_*/z_t$. This expression can be inverted numerically to obtain $x(a)$.[22]

_____

[22]Note that the energy conservation equation $d\rho_d/dt + 3H(\rho_d + p_d) = 0$ in the dark sector is also automatically satisfied in this case. We can rewrite it as $a \frac{dx}{da}\frac{d\rho_d}{dx} = -3(\rho_d + p_d)$. Writing the entropy equation as $x(\rho_d + p_d) \propto 1/a^3$ and taking a derivative of this equation with respect to a, one can check that energy conservation requires that $\rho_d + p_d + x\frac{dp_d}{dx} = 0$. This is satisfied for the contribution from gauge bosons. For the Higgs, it requires $\hat{\rho} - \hat{p} + \frac{x}{3}\frac{d\hat{p}}{dx} = 0$. Using explicit expressions from above, one sees that this is indeed satisfied.

[1] E. Abdalla *et al.*, Cosmology intertwined: A review of the particle physics, astrophysics, and cosmology associated with the cosmological tensions and anomalies, J. High Energy Astrophys. **34,** 49 (2022).

[2] A. G. Riess, G. S. Anand, W. Yuan, S. Casertano, A. Dolphin, L. M. Macri, L. Breuval, D. Scolnic, M. Perrin, and I. R. Anderson, JWST observations reject unrecognized crowding of cepheid photometry as an explanation for the Hubble tension at 8σ confidence, Astrophys. J. Lett. **962,** L17 (2024).

[3] J. L. Bernal, L. Verde, and A. G. Riess, The trouble with H_0, J. Cosmol. Astropart. Phys. 10 (2016) 019.

[4] L. Knox and M. Millea, Hubble constant hunter's guide, Phys. Rev. D **101,** 043533 (2020).

[5] M. A. Buen-Abad, G. Marques-Tavares, and M. Schmaltz, Non-Abelian dark matter and dark radiation, Phys. Rev. D **92,** 023531 (2015).

[6] M. A. Buen-Abad, M. Schmaltz, J. Lesgourgues, and T. Brinckmann, Interacting dark sector and precision cosmology, J. Cosmol. Astropart. Phys. 01 (2018) 008.

[7] M. Archidiacono, S. Gariazzo, C. Giunti, S. Hannestad, and T. Tram, Sterile neutrino self-interactions: H_0 tension and short-baseline anomalies, J. Cosmol. Astropart. Phys. 12 (2020) 029.

[8] D. Aloni, A. Berlin, M. Joseph, M. Schmaltz, and N. Weiner, A step in understanding the Hubble tension, Phys. Rev. D **105,** 123516 (2022).

[9] N. Schöneberg and G. Franco Abellán, A step in the right direction? Analyzing the Wess Zumino dark radiation solution to the Hubble tension, J. Cosmol. Astropart. Phys. 12 (2022) 001.

[10] M. A. Buen-Abad, Z. Chacko, C. Kilic, G. Marques-Tavares, and T. Youn, Stepped partially acoustic dark matter, large scale structure, and the Hubble tension, J. High Energy Phys. 06 (2023) 012.

[11] I. J. Allali, F. Rompineve, and M. P. Hertzberg, Dark sectors with mass thresholds face cosmological datasets, Phys. Rev. D **108,** 023527 (2023).

[12] A. Berlin and N. Blinov, Thermal dark matter below an MeV, Phys. Rev. Lett. **120,** 021801 (2018).

[13] M. Berbig, S. Jana, and A. Trautner, The Hubble tension and a renormalizable model of gauged neutrino self-interactions, Phys. Rev. D **102,** 115008 (2020).

[14] M. Escudero, T. Schwetz, and J. Terol-Calvo, A seesaw model for large neutrino masses in concordance with cosmology, J. High Energy Phys. 02 (2023) 142.

[15] D. Aloni, M. Joseph, M. Schmaltz, and N. Weiner, Dark radiation from neutrino mixing after big bang nucleosynthesis, Phys. Rev. Lett. **131,** 221001 (2023).

[16] F. Niedermann and M. S. Sloth, Hot new early dark energy, Phys. Rev. D **105,** 063509 (2022).

[17] F. Niedermann and M. S. Sloth, Hot new early dark energy: Towards a unified dark sector of neutrinos, dark energy and dark matter, Phys. Lett. B **835,** 137555 (2022).

[18] E. Witten, Cosmological consequences of a light Higgs boson, Nucl. Phys. **B177,** 477 (1981).

[19] S. R. Coleman and E. J. Weinberg, Radiative corrections as the origin of spontaneous symmetry breaking, Phys. Rev. D **7,** 1888 (1973).

[20] F. Niedermann and M. S. Sloth, New early dark energy, Phys. Rev. D **103,** L041303 (2021).

[21] F. Niedermann and M. S. Sloth, Resolving the Hubble tension with new early dark energy, Phys. Rev. D **102,** 063527 (2020).

[22] F. Niedermann and M. S. Sloth, New early dark energy as a solution to the H_0 and S_8 tensions, in *The Hubble Constant Tension*, edited by E. di Valentino and D. Brout (Springer, Singapore, 2024).

[23] V. Poulin, T. L. Smith, T. Karwal, and M. Kamionkowski, Early dark energy can resolve the Hubble tension, Phys. Rev. Lett. **122,** 221301 (2019).

[24] V. Poulin, T. L. Smith, and T. Karwal, The ups and downs of early dark energy solutions to the Hubble tension: A review of models, hints and constraints circa 2023, Phys. Dark Universe **42,** 101348 (2023).

[25] J. S. Cruz, F. Niedermann, and M. S. Sloth, NANOGrav meets hot new early dark energy and the origin of neutrino mass, Phys. Lett. B **846,** 138202 (2023).

[26] J. S. Cruz, F. Niedermann, and M. S. Sloth, Cold new early dark energy pulls the trigger on the H_0 and S_8 tensions: A simultaneous solution to both tensions without new ingredients, J. Cosmol. Astropart. Phys. 11 (2023) 033.

[27] W. Fischler and J. Meyers, Dark radiation emerging after big bang nucleosynthesis?, Phys. Rev. D **83,** 063520 (2011).

[28] D. Hooper, F. S. Queiroz, and N. Y. Gnedin, Non-thermal dark matter mimicking an additional neutrino species in the early universe, Phys. Rev. D **85,** 063513 (2012).

[29] O. E. Bjaelde, S. Das, and A. Moss, Origin of Delta $N_{\rm eff}$ as a result of an interaction between dark radiation and dark matter, J. Cosmol. Astropart. Phys. 10 (2012) 017.

[30] K. Choi, K.-Y. Choi, and C. S. Shin, Dark radiation and small-scale structure problems with decaying particles, Phys. Rev. D **86,** 083529 (2012).

[31] A. Nygaard, E. B. Holm, T. Tram, and S. Hannestad, Decaying dark matter and the Hubble tension, arXiv:2307.00418.

[32] T.-H. Yeh, J. Shelton, K. A. Olive, and B. D. Fields, Probing physics beyond the standard model: Limits from BBN and the CMB independently and combined, J. Cosmol. Astropart. Phys. 10 (2022) 046.

[33] N. Schöneberg, The 2024 BBN baryon abundance update, J. Cosmol. Astropart. Phys. 06 (2024) 006.

[34] D. Baumann, D. Green, and B. Wallisch, Searching for light relics with large-scale structure, J. Cosmol. Astropart. Phys. 08 (2018) 029.

[35] M. Archidiacono, S. Hannestad, R. S. Hansen, and T. Tram, Cosmology with self-interacting sterile neutrinos and dark matter—A pseudoscalar model, Phys. Rev. D **91,** 065021 (2015).

[36] S.-P. Li and X.-J. Xu, Production rates of dark photons and Z' in the Sun and stellar cooling bounds, J. Cosmol. Astropart. Phys. 09 (2023) 009.

[37] K. Yamamoto, Phase transition associated with intermediate gauge symmetry breaking in superstring models, Phys. Lett. **168B,** 341 (1986).

[38] T. Barreiro, E. J. Copeland, D. H. Lyth, and T. Prokopec, Some aspects of thermal inflation: The finite temperature

potential and topological defects, Phys. Rev. D **54,** 1379 (1996).

[39] E. Gildener and S. Weinberg, Symmetry breaking and scalar bosons, Phys. Rev. D **13,** 3333 (1976).

[40] S. Iso, P. D. Serpico, and K. Shimada, QCD-electroweak first-order phase transition in a supercooled universe, Phys. Rev. Lett. **119,** 141301 (2017).

[41] N. Levi, T. Opferkuch, and D. Redigolo, The supercooling window at weak and strong coupling, J. High Energy Phys. 02 (2023) 125.

[42] A. Salvio, Supercooling in radiative symmetry breaking: Theory extensions, gravitational wave detection and primordial black holes, J. Cosmol. Astropart. Phys. 12 (2023) 046.

[43] M. Kierkla, B. Swiezewska, T. V. I. Tenkanen, and J. van de Vis, Gravitational waves from supercooled phase transitions: dimensional transmutation meets dimensional reduction, J. High Energy Phys. 02 (2024) 234.

[44] K. Freese and M. W. Winkler, Dark matter and gravitational waves from a dark big bang, Phys. Rev. D **107,** 083522 (2023).

[45] A. H. Guth and E. J. Weinberg, Could the universe have recovered from a slow first order phase transition?, Nucl. Phys. **B212,** 321 (1983).

[46] L. Dolan and R. Jackiw, Symmetry behavior at finite temperature, Phys. Rev. D **9,** 3320 (1974).

[47] M. Dine, R. G. Leigh, P. Y. Huet, A. D. Linde, and D. A. Linde, Towards the theory of the electroweak phase transition, Phys. Rev. D **46,** 550 (1992).

[48] P. B. Arnold and O. Espinosa, The Effective potential and first order phase transitions: Beyond leading-order, Phys. Rev. D **47,** 3546 (1993); **50,** 6662(E) (1994).

[49] O. Gould and T. V. I. Tenkanen, On the perturbative expansion at high temperature and implications for cosmological phase transitions, J. High Energy Phys. 06 (2021) 069.

[50] D. Bodeker and G. D. Moore, Can electroweak bubble walls run away?, J. Cosmol. Astropart. Phys. 05 (2009) 009.

[51] D. Bodeker and G. D. Moore, Electroweak bubble wall speed limit, J. Cosmol. Astropart. Phys. 05 (2017) 025.

[52] P. Athron, C. Balázs, and L. Morris, Supercool subtleties of cosmological phase transitions, J. Cosmol. Astropart. Phys. 03 (2023) 006.

[53] J. Ellis, M. Lewicki, and V. Vaskonen, Updated predictions for gravitational waves produced in a strongly supercooled phase transition, J. Cosmol. Astropart. Phys. 11 (2020) 020.

[54] Y. Gouttenoire, R. Jinno, and F. Sala, Friction pressure on relativistic bubble walls, J. High Energy Phys. 05 (2022) 004.

[55] R. Jinno, T. Konstandin, and H. Rubira, A hybrid simulation of gravitational wave production in first-order phase transitions, J. Cosmol. Astropart. Phys. 04 (2021) 014.

[56] R. Jinno, T. Konstandin, H. Rubira, and J. van de Vis, Effect of density fluctuations on gravitational wave production in first-order phase transitions, J. Cosmol. Astropart. Phys. 12 (2021) 019.

[57] R. Jinno, T. Konstandin, H. Rubira, and I. Stomberg, Higgsless simulations of cosmological phase transitions

and gravitational waves, J. Cosmol. Astropart. Phys. 02 (2023) 011.

[58] M. Hindmarsh, S. J. Huber, K. Rummukainen, and D. J. Weir, Gravitational waves from the sound of a first order phase transition, Phys. Rev. Lett. **112,** 041301 (2014).

[59] M. Hindmarsh, S. J. Huber, K. Rummukainen, and D. J. Weir, Numerical simulations of acoustically generated gravitational waves at a first order phase transition, Phys. Rev. D **92,** 123009 (2015).

[60] M. Hindmarsh, Sound shell model for acoustic gravitational wave production at a first-order phase transition in the early Universe, Phys. Rev. Lett. **120,** 071301 (2018).

[61] M. Hindmarsh, S. J. Huber, K. Rummukainen, and D. J. Weir, Shape of the acoustic gravitational wave power spectrum from a first order phase transition, Phys. Rev. D **96,** 103520 (2017); **101,** 089902(E) (2020).

[62] C. Caprini, R. Durrer, and G. Servant, The stochastic gravitational wave background from turbulence and magnetic fields generated by a first-order phase transition, J. Cosmol. Astropart. Phys. 12 (2009) 024.

[63] D. Cutting, M. Hindmarsh, and D. J. Weir, Vorticity, kinetic energy, and suppressed gravitational wave production in strong first order phase transitions, Phys. Rev. Lett. **125,** 021302 (2020).

[64] P. Auclair, C. Caprini, D. Cutting, M. Hindmarsh, K. Rummukainen, D. A. Steer, and D. J. Weir, Generation of gravitational waves from freely decaying turbulence, J. Cosmol. Astropart. Phys. 09 (2022) 029.

[65] C. Caprini and D. G. Figueroa, Cosmological backgrounds of gravitational waves, Classical Quantum Gravity **35,** 163001 (2018).

[66] W. J. Marciano, C. Zhang, and S. Willenbrock, Higgs decay to two photons, Phys. Rev. D **85,** 013002 (2012).

[67] M. Garny, A. Palessandro, M. Sandora, and M. S. Sloth, Charged Planckian interacting dark matter, J. Cosmol. Astropart. Phys. 01 (2019) 021.

[68] A. Kurkela and E. Lu, Approach to equilibrium in weakly coupled non-Abelian plasmas, Phys. Rev. Lett. **113,** 182301 (2014).

[69] M. C. Abraao York, A. Kurkela, E. Lu, and G. D. Moore, UV cascade in classical Yang-Mills theory via kinetic theory, Phys. Rev. D **89,** 074036 (2014).

[70] M.-X. Lin, G. Benevento, W. Hu, and M. Raveri, Acoustic dark energy: Potential conversion of the Hubble tension, Phys. Rev. D **100,** 063542 (2019).

[71] G. Elor, R. Jinno, S. Kumar, R. McGehee, and Y. Tsai, Finite bubble statistics constrain late cosmological phase transitions, arXiv:2311.16222.

[72] N. Deruelle and V. F. Mukhanov, On matching conditions for cosmological perturbations, Phys. Rev. D **52,** 5549 (1995).

[73] W. Israel, Singular hypersurfaces and thin shells in general relativity, Nuovo Cim. B **44,** 1 (1966); **48,** 463(E) (1967).

[74] C.-P. Ma and E. Bertschinger, Cosmological perturbation theory in the synchronous and conformal Newtonian gauges, Astrophys. J. **455,** 7 (1995).

[75] W. Hu, Structure formation with generalized dark matter, Astrophys. J. **506,** 485 (1998).

[76] D. Blas, J. Lesgourgues, and T. Tram, The cosmic linear anisotropy solving system (CLASS) II: Approximation schemes, J. Cosmol. Astropart. Phys. 07 (2011) 034.

[77] B. Audren, J. Lesgourgues, K. Benabed, and S. Prunet, Conservative constraints on early cosmology: An illustration of the Monte Python cosmological parameter inference code, J. Cosmol. Astropart. Phys. 02 (2013) 001.

[78] T. Brinckmann and J. Lesgourgues, MontePython 3: Boosted MCMC sampler and other features, Phys. Dark Universe **24,** 100260 (2019).

[79] O. Pisanti, A. Cirillo, S. Esposito, F. Iocco, G. Mangano, G. Miele, and P. D. Serpico, PArthENoPE: Public algorithm evaluating the nucleosynthesis of primordial elements, Comput. Phys. Commun. **178,** 956 (2008).

[80] N. Aghanim et al. (Planck Collaboration), Planck 2018 results. VI. Cosmological parameters, Astron. Astrophys. **641,** A6 (2020); **652,** C4(E) (2021).

[81] N. Aghanim et al. (Planck Collaboration), Planck 2018 results. VIII. Gravitational lensing, Astron. Astrophys. **641,** A8 (2020).

[82] F. Beutler, C. Blake, M. Colless, D. H. Jones, L. Staveley-Smith, L. Campbell, Q. Parker, W. Saunders, and F. Watson, The 6dF galaxy survey: Baryon acoustic oscillations and the local Hubble constant, Mon. Not. R. Astron. Soc. **416,** 3017 (2011).

[83] A. J. Ross, L. Samushia, C. Howlett, W. J. Percival, A. Burden, and M. Manera, The clustering of the SDSS DR7 main Galaxy sample—I. A 4 per cent distance measure at $z = 0.15$, Mon. Not. R. Astron. Soc. **449,** 835 (2015).

[84] S. Alam et al. (BOSS Collaboration), The clustering of galaxies in the completed SDSS-III Baryon Oscillation Spectroscopic Survey: Cosmological analysis of the DR12 galaxy sample, Mon. Not. R. Astron. Soc. **470,** 2617 (2017).

[85] D. M. Scolnic et al. (Pan-STARRS1 Collaboration), The complete light-curve sample of spectroscopically confirmed SNe Ia from Pan-STARRS1 and cosmological constraints from the combined Pantheon sample, Astrophys. J. **859,** 101 (2018).

[86] A. G. Riess et al., A comprehensive measurement of the local value of the Hubble constant with 1 km s^{-1} Mpc^{-1} uncertainty from the Hubble Space Telescope and the SH0ES Team, Astrophys. J. Lett. **934,** L7 (2022).

[87] M. Raveri and W. Hu, Concordance and discordance in cosmology, Phys. Rev. D **99,** 043506 (2019).

[88] A. R. Liddle, Information criteria for astrophysical model selection, Mon. Not. R. Astron. Soc. **377,** L74 (2007).

[89] N. Schöneberg, G. Franco Abellán, A. Pérez Sánchez, S. J. Witte, V. Poulin, and J. Lesgourgues, The H0 Olympics: A fair ranking of proposed models, Phys. Rep. **984,** 1 (2022).

[90] M. Joseph, D. Aloni, M. Schmaltz, E. N. Sivarajan, and N. Weiner, A step in understanding the S8 tension, Phys. Rev. D **108,** 023520 (2023).

[91] N. Schöneberg, G. Franco Abellán, T. Simon, A. Bartlett, Y. Patel, and T. L. Smith, Comparative analysis of interacting stepped dark radiation, Phys. Rev. D **108,** 123513 (2023).

[92] A. R. Khalife, M. B. Zanjani, S. Galli, S. Günther, J. Lesgourgues, and K. Benabed, Review of Hubble tension solutions with new sh0es and spt-3g data, J. Cosmol. Astropart. Phys. 04 (2024) 059.

[93] C. García-García, M. Zennaro, G. Aricò, D. Alonso, and R. E. Angulo, Cosmic shear with small scales: DES-Y3, KiDS-1000 and HSC-DR1, arXiv:2403.13794.

[94] S. J. Huber and T. Konstandin, Gravitational wave production by collisions: More bubbles, J. Cosmol. Astropart. Phys. 09 (2008) 022.

[95] C. Caprini, R. Durrer, and G. Servant, Gravitational wave generation from bubble collisions in first-order phase transitions: An analytic approach, Phys. Rev. D **77,** 124015 (2008).

[96] C. Caprini, R. Durrer, T. Konstandin, and G. Servant, General properties of the gravitational wave spectrum from phase transitions, Phys. Rev. D **79,** 083519 (2009).

[97] D. J. Weir, Revisiting the envelope approximation: Gravitational waves from bubble collisions, Phys. Rev. D **93,** 124037 (2016).

[98] R. Jinno and M. Takimoto, Gravitational waves from bubble collisions: An analytic derivation, Phys. Rev. D **95,** 024009 (2017).

[99] R. Jinno and M. Takimoto, Gravitational waves from bubble dynamics: Beyond the envelope, J. Cosmol. Astropart. Phys. 01 (2019) 060.

[100] T. Konstandin, Gravitational radiation from a bulk flow model, J. Cosmol. Astropart. Phys. 03 (2018) 047.

[101] C. J. Moore, R. H. Cole, and C. P. L. Berry, Gravitational-wave sensitivity curves, Classical Quantum Gravity **32,** 015014 (2015).

[102] C. L. Carilli and S. Rawlings, Science with the square kilometer array: Motivation, key science projects, standards and assumptions, New Astron. Rev. **48,** 979 (2004).

[103] G. Janssen et al., Gravitational wave astronomy with the SKA, Proc. Sci., AASKA14 (2015) 037 [arXiv:1501.00127].

[104] A. Weltman et al., Fundamental physics with the square kilometre array, Pub. Astron. Soc. Aust. **37,** e002 (2020).

[105] G. Agazie et al. (NANOGrav Collaboration), The NANOGrav 15 yr data set: Evidence for a gravitational-wave background, Astrophys. J. Lett. **951,** L8 (2023).

[106] T. Bringmann, P. F. Depta, T. Konstandin, K. Schmidt-Hoberg, and C. Tasillo, Does NANOGrav observe a dark sector phase transition?, J. Cosmol. Astropart. Phys. 11 (2023) 053.

[107] D. Cutting, M. Hindmarsh, and D. J. Weir, Gravitational waves from vacuum first-order phase transitions: From the envelope to the lattice, Phys. Rev. D **97,** 123513 (2018).

[108] D. Cutting, E. G. Escartin, M. Hindmarsh, and D. J. Weir, Gravitational waves from vacuum first order phase transitions II: from thin to thick walls, Phys. Rev. D **103,** 023531 (2021).

[109] DESI Collaboration, The DESI experiment part I: Science, targeting, and survey design, arXiv:1611.00036.

[110] N. G. Karaçaylı, A. Font-Ribera, and N. Padmanabhan, Optimal 1D Ly α forest power spectrum estimation—I. DESI-lite spectra, Mon. Not. R. Astron. Soc. **497,** 4742 (2020).

[111] M. Walther, E. Armengaud, C. Ravoux, N. Palanque-Delabrouille, C. Yèche, and Z. Lukić, Simulating

intergalactic gas for DESI-like small scale Lymanα forest observations, J. Cosmol. Astropart. Phys. 04 (2021) 059.

[112] N. G. Karaçaylı *et al.*, Optimal 1D Lyα Forest power spectrum estimation—III. DESI early data, Mon. Not. R. Astron. Soc. **528,** 3941 (2024).

[113] H. Rubira, A. Mazoun, and M. Garny, Full-shape BOSS constraints on dark matter interacting with dark radiation and lifting the S_8 tension, J. Cosmol. Astropart. Phys. 01 (2023) 034.

[114] A. Mazoun, S. Bocquet, M. Garny, J. J. Mohr, H. Rubira, and S. M. L. Vogt, Probing interacting dark sector models with future weak lensing-informed galaxy cluster abundance constraints from SPT-3G and CMB-S4, Phys. Rev. D **109,** 063536 (2024).

[115] M. Garny, M. Sandora, and M. S. Sloth, Planckian interacting massive particles as dark matter, Phys. Rev. Lett. **116,** 101302 (2016).